AD-A124 675   ELECTRICAL PROPERTIES OF SILICON-IMPLANTED GAAS(U) AIR   1/1
FORCE INST OF TECH WRIGHT-PATTERSON AFB OH SCHOOL OF
ENGINEERING Y Y KIM DEC 82 AFIT/GEP/PH/82D-17
UNCLASSIFIED   F/G 20/12   NL

END

FILMED

DTIC

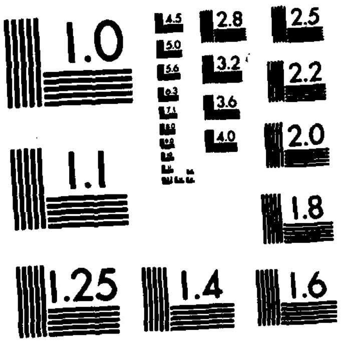

MICROCOPY RESOLUTION TEST CHART
NATIONAL BUREAU OF STANDARDS-1963-A

ELECTRICAL PROPERTIES
OF SILICON-IMPLANTED GaAs

THESIS

Yong Yun Kim
Captain ROKA

AFIT/GEP/PH/82D-17

DEPARTMENT OF THE AIR FORCE
AIR UNIVERSITY (ATC)
AIR FORCE INSTITUTE OF TECHNOLOGY

Wright-Patterson Air Force Base, Ohio

AFIT/GEP/PH/82D-17

ELECTRICAL PROPERTIES
OF SILICON-IMPLANTED GaAs

THESIS

AFIT/GEP/PH/82D-17

Yong Yun Kim
Captain ROKA

Approved for Public Release; Distribution Unlimited

AFIT/GEP/PH/82D-17

ELECTRICAL PROPERTIES
OF SILICON-IMPLANTED GaAs

THESIS

Presented to the Faculty of the School of Engineering
of the Air Force Institute of Technology
Air University
in Partial Fulfillment of the
Requirements for the Degree of
Master of Science

by
Yong Yun Kim, B.S.
Captain ROKA
Graduate Engineering Physics
December 1982

Preface

This study was sponsored by the Electronic Research Branch of the Air Force Avionics Laboratory, Wright-Patterson Air Force Base, Ohio. It is a part of their continuing investigation into the electrical and physical properties of ion implanted GaAs. The work, a study of electrical properties of Si-implanted GaAs, has been done in support of work being performed at this laboratory and with outside contracts.

I wish to express my sincere thanks to a great number of people for their guidance and help during this investigation. I especially want to thank Dr. Y. K. Yeo for his invaluable guidance and assistance. I also would like to thank Professor R. L. Hengehold, who is my thesis advisor, Dr. Y. S. Park, J. Ehret for performing the ion implantation, and C. Geesner for depositing the encapsulants. Finally I wish to extend my thanks to my wife, Min Ju, for her emotional and secretarial support throughout this undertaking.

Yong Yun Kim

(This thesis was typed by Diane M. Katterheinrich)

Contents

List of Figures

List of Figures

List of Tables

AFIT/GEP/PH/82D-17

Abstract

A comprehensive study of the electrical properties of low-dose Si implants in both Cr-doped and undoped GaAs substrates has been made using the Hall-effect/sheet-resistivity measurement technique for various ion doses, ion energies, and annealing temperatures. The samples were implanted at room temperature and annealed with silicon nitride encapsulants in a hydrogen atmosphere for 15 minutes. N-type layers were produced at all dose levels investigated, and the optimum annealing temperature was 850°C for all doses. The highest electrical activation efficiencies obtained were 89% and 87% for Cr-doped and undoped GaAs substrates, respectively. The electrical activations and mobilities of undoped GaAs are, in general, higher than those of Cr-doped GaAs at all annealing temperatures for a given dose. The electrical activations and mobilities also depend upon the ion energy, ~~and they~~ increase ing with ion energy. Depth profiles of carrier concentrations and mobilities are highly dependent upon ion dose and annealing temperature. In general, the carrier profiles do not follow the theoretical profiles. The carrier profiles for undoped GaAs are much broader than those for Cr-doped GaAs. Significant implantation damage still remains after an 800°C anneal, and a 900°C anneal produces significant outdiffusion as well as indiffusion of the implanted Si ions.

ELECTRICAL PROPERTIES
OF SILICON-IMPLANTED GaAs

I. Introduction

In recent years, ion implantation directly into semi-insulating GaAs substrates has been used for the fabrication of various devices such as field effect transistors (FETs) and integrated circuits (ICs). In particular, silicon-implanted GaAs has been widely used, because Si is a light atom and hence it has sufficient ion range for many device requirements. Moreover, it has been found that, for low dose Si implants, high electrical activation efficiencies (surface carrier concentration divided by the implanted ion dose) are generally achieved with room temperature implantation (Ref 1), while with other n-type dopants such as S and Se, it is generally more difficult to achieve high electrical activation with room temperature implantation (Refs 2,3).

Si, like Ge, is an amphoteric dopant in GaAs; therefore, theoretically, it should be possible to produce n- or p-type conductivity. However, the implanted Si has been found to be an n-type dopant in GaAs (Refs 4, 5, 6), which implies that the implanted Si ions preferentially go into Ga sites.

Although a number of publications (Refs 1, 4, 5, 7) dealing with the electrical properties of Si implants in GaAs have appeared in the literature, the fundamental difficulties encountered with this dopant are still not well understood. In particular, no comprehensive study has been made for low dose Si implants in GaAs in spite of the wide use of the low dose in device fabrication. Moreover, there are inconsistent reports about depth profiles of electrical carrier concentrations and diffusion of Si during annealing. Most studies have been made using Cr-doped semi-insulating GaAs but only a few studies have been done using undoped semi-insulating GaAs.

Thesis Objective and Scope

The objective of this thesis was the characterization of the electrical properties of Si-ion-implanted GaAs in the low dose range, and thereby the attainment of useful information for device applications. In order to better understand the factors affecting electrical activation and carrier depth distribution, a comprehensive study of GaAs:Si was undertaken. Optimum annealing temperatures that produce maximum electrical activation were determined for each dose. Since the device performance may strongly depend upon the shape of the carrier profile, net carrier concentration, and mobility, depth profiles of carriers and mobilities were also made for each dose at the optimum annealing temperature.

The substrate materials used were <100> oriented Cr-doped and undoped semi-insulating GaAs. Ion implantation was carried out at room temperature at an ion energy of 100 keV. The doses used were 1×10^{12}, 2×10^{12}, 3×10^{12}, 4×10^{12}, 6×10^{12}, 8×10^{12}, and 1×10^{13} cm^{-2}. Samples were also implanted with a dose of 4×10^{12} cm^{-2} at various ion energies ranging from 50 to 375 keV. As a protective mechanism during the annealing of the samples, a pyrolytic Si_3N_4 encapsulant was used. The samples were annealed at 800, 850, and 900°C. The sheet resistivity and Hall coefficient of each sample were measured using the van der Pauw technique (Refs 8, 9, 10, 11). Depth profiles of carrier concentration and Hall mobility were measured by the combined use of Hall measurements and the chemical layer-removal technique.

Sequence of Presentation

Chapter II provides background information for this study. It contains the basic concepts and problems of ion implantation. A brief description of ion-range statistics is also given in this chapter. Chapter III describes detailed experimental procedures, sample preparation procedures before and after ion implantation, a criteria for GaAs substrate selection, a description of the Hall-measurement system, and the electrical measurement methods. The experimental results of Si-implanted GaAs and the discussion of these results are presented in Chapter IV. Electrical activation and carrier profile dependence upon ion dose and annealing temperature are described for both Cr-doped and undoped substrates, and these results are compared with each other. Chapter V concludes this study with a summary of significant results and with some suggestions for further study. The appendix includes a table of ion-range statistics for Si implants in GaAs.

II. Background

Ion Implantation

The electronic and optical properties of semiconductor materials can be changed by introducing appropriate impurities into semiconductors. This process, called "doping", involves the introduction of a desired impurity atom onto a lattice site in the host crystal. Conventionally, this is achieved either during the crystal growth process or by thermal diffusion. An alternative process is that of ion implantation, where the desired impurities are injected into semiconductors using an energetic ion beam.

The ion implantation technique has advantages over the conventional technologies. It offers accurate control of impurity concentration and profile, good reproducibility, only slight lateral spreading, and the ability to achieve doping profiles not easily obtained by other techniques. Also, ion implantation can be done at relatively low temperatures, and this is especially useful for the doping of compound semiconductors.

In spite of the many advantages of introducing impurities by the ion implantation technique, many problems also exist. Undesirable crystalline defects are produced during the injection of dopants into a semiconductor using an energetic ion beam. Also, the ions do not all settle in substitutional lattice sites. Therefore, the implanted ions do not all become electrically active and thermal annealing is required to remove the radiation damage, to bring the dopants into electrically active sites, and to re-order the crystal. In general, high annealing temperatures (700°C to 950°C) are required to achieve maximum electrical activation of the implanted ions. However, dopants and/or substrate elements can be lost during thermal annealing. Therefore, some kind of surface protection, that is, an encapsulant, is required to prevent any loss of the dopant or the host atoms during high temperature annealing.

Lindhard, Scharff and Schiott (LSS) Theory

The LSS theory describes the distribution of implanted ions with depth in an amorphous solid. When an energetic ion enters a solid, it suffers collisions, losing energy either to the target-atom's nuclei or electrons, resulting in the consequent deflection from its original trajectory until it is finally brought to rest. If the target material is amorphous, then the stopping process for any particular ion of an incident monoenergetic beam will be random, and the distribution of implanted ions can be shown to be approximately Gaussian, characterized by an average projected range and a standard deviation (Ref 12: 44).

In crystalline targets, the distribution of implanted ions is dependent on the orientation of the substrate during the implantation. If the incident beam is aligned with one of the major crystal axes or planes, then the phenomenon of channeling may take place whereby some of the implanted ions penetrate to depths far greater than predicted for amorphous targets. This problem can generally be minimized by misaligning the target crystal so that the ion beam is incident in a nonchanneling direction, thus making the target material appear amorphous (Refs 12, 13).

The LSS theory considers the effect of the stopping power of the atoms in the substrate on the implanted ions through various kinetic energy loss mechanism. The result is a Gaussian distribution in which the average projected range, R_p , the position of the peak of the distribution and its standard deviation, σ_p , depend upon the energy, as well as the atomic number of the implanted ions and that of the substrate. Gibbons et al (Ref 14) have developed a computer program to calculate R_p and σ_p and have tabulated the results for various energies, implanted ions, and substrates.

The concentration, $N(x_p)$, of the implanted ions as a function of the distance from the substrate surface can be obtained by

$$N(x_p) = \frac{\phi}{\sigma_p \sqrt{2\pi}} \text{ EXP } \left[- \frac{(x_p - R_p)^2}{2\,\sigma_p^2}\right] , \qquad (1)$$

where x_p is the depth measured along the direction of incidence of the beam in Å, ϕ is the fluence, or ion dose per cm^2, R_p is the projected range in Å, and σ_p is the standard deviation of the projected range in Å. The resulting profile will be similar to the theoretical distribution shown in Figure 1.

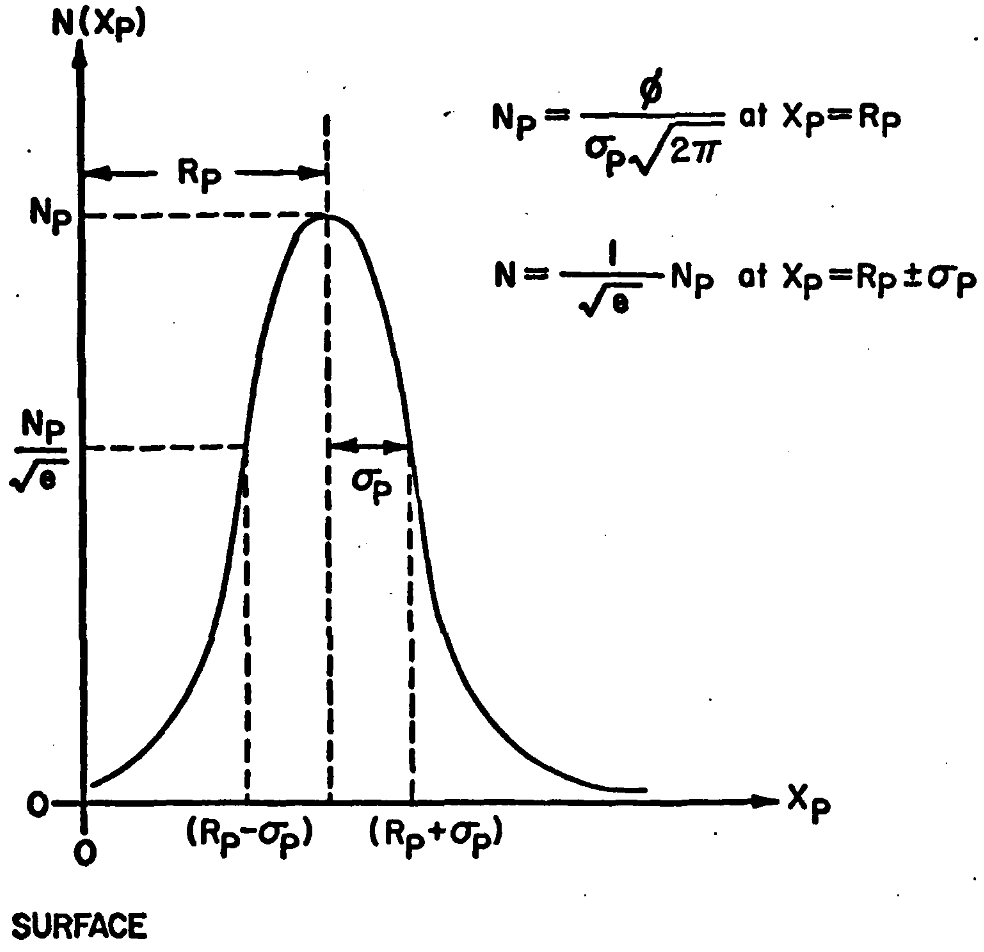

Figure 1. Typical Theoretical Gaussian Ion Distribution

III. Experimental Procedures

Sample Preparation

The substrate materials used for this study were <100> oriented Cr-doped and undoped semi-insulating GaAs single crystals, obtained from Crystal Specialties, Inc. and Cambridge Instruments, Ltd., respectively. The substrate wafers were scribed and broken into the square-shaped samples about 0.5 cm on a side. Prior to implantation, the samples were carefully cleaned with 10% aquasol, de-ionized water, trichloroethylene, acetone, and methanol, and were dried with nitrogen gas. They were subsequently free-etched with an $H_2SO:30\%H_2O_2:H_2O$ solution in a 3:1:1 ratio by volume for 60 seconds. Room temperature implantation was carried out at an energy of 100 keV to doses ranging from 1×10^{12} to 1×10^{13} cm^{-2}. The incident-ion beam was directed 7° off the <100> crystal axis to minimize ion-channeling effects. After implantation, the samples were carefully cleaned again just before capping with an $\sim$1000 Å layer of Si_3N_4 pyrolytically deposited at $\sim$700° C for 30 seconds. The samples were then annealed in flowing hydrogen gas for 15 minutes at 800, 850, and 900° C. The encapsulants were removed with a 48% hydrofluoric acid after annealing, usually requiring about 3 $\sim$ 5 minutes immersion for Si_3N_4 films. The samples were rinsed in flowing de-ionized water and blown dry with nitrogen gas. Electrical indium contacts were made on the four corners of the square-shaped implanted surface using an ultrasonic soldering iron. The contacts were then heated at 350° C for 3 minutes in flowing argon gas to produce ohmic behavior. Ohmicity of the contacts was checked using a curve tracer.

Substrate Qualification Test

Thermal conversion is a process which results in the formation of a conducting layer in the vicinity of the surface of a semi-insulating substrate when it is annealed at high temperature. This thermal conversion seriously affects the electrical behavior of the implanted samples. Therefore, thermal conversion tests were made for several semi-insulating GaAs substrates before ion implantation in order to select good substrates. The substrates were free-etched, capped with pyrolytic Si_3N_4 encapsulants, and annealed at 900° C for 15 minutes in flowing hydrogen gas. The results of Hall measurements of various substrates are shown in Table I. Among the tested samples, CS-E-119 (Cr-doped) and MR-A001/R3 (undoped), were chosen for low-dose Si implantation.

Electrical Measurements

Hall-effect/sheet-resistivity measurements were made using the standard van der Pauw technique and an apparatus which is suitable for high-resistivity measurements.

The van der Pauw technique requires only four contacts

Table I

Typical Results of Substrate Qualification Test

Substrate Number	Kind of Substrates	Sheet Resistivity (Ω/□)	Number of Carriers (cm^{-2})	Types of Conductivity
CS-E-119	Cr-doped	2.8×10^6	8.1×10^9	No-type
CS-E-159	Cr-doped	6.7×10^5	4.3×10^{10}	No-type
CS-E-222	Cr-doped	1.3×10^3	1.1×10^{12}	N
CS-E-647	Cr-doped	8.7×10^2	1.6×10^{12}	N
CS-E-1120	Cr-doped	4.2×10^4	3.4×10^{11}	N
CS-E-1600	Cr-doped	4.9×10^4	4.1×10^{10}	N
A245R/ID	Undoped	2.6×10^7	2.2×10^{10}	No-type
MR-A001/R3	Undoped	2.3×10^6	3.7×10^{10}	P
MR-A540	Undoped	2.8×10^4	6.8×10^{11}	P
MR-A555	Undoped	1.1×10^4	1.2×10^{11}	N

located anywhere on the periphery of a uniformly thick sample of arbitrary shape. However, it is necessary to measure voltages and currents across different pairs of contacts in order to correct for the geometry, which requires interchanging current and voltage leads to the sample as shown schematically in Figure 2. In each of the six configurations illustrated in Figure 2, the current and the voltage between V1 and V2 are recorded. In position (e) and (f), the voltage between V1 and V2 is measured with the magnetic field applied.

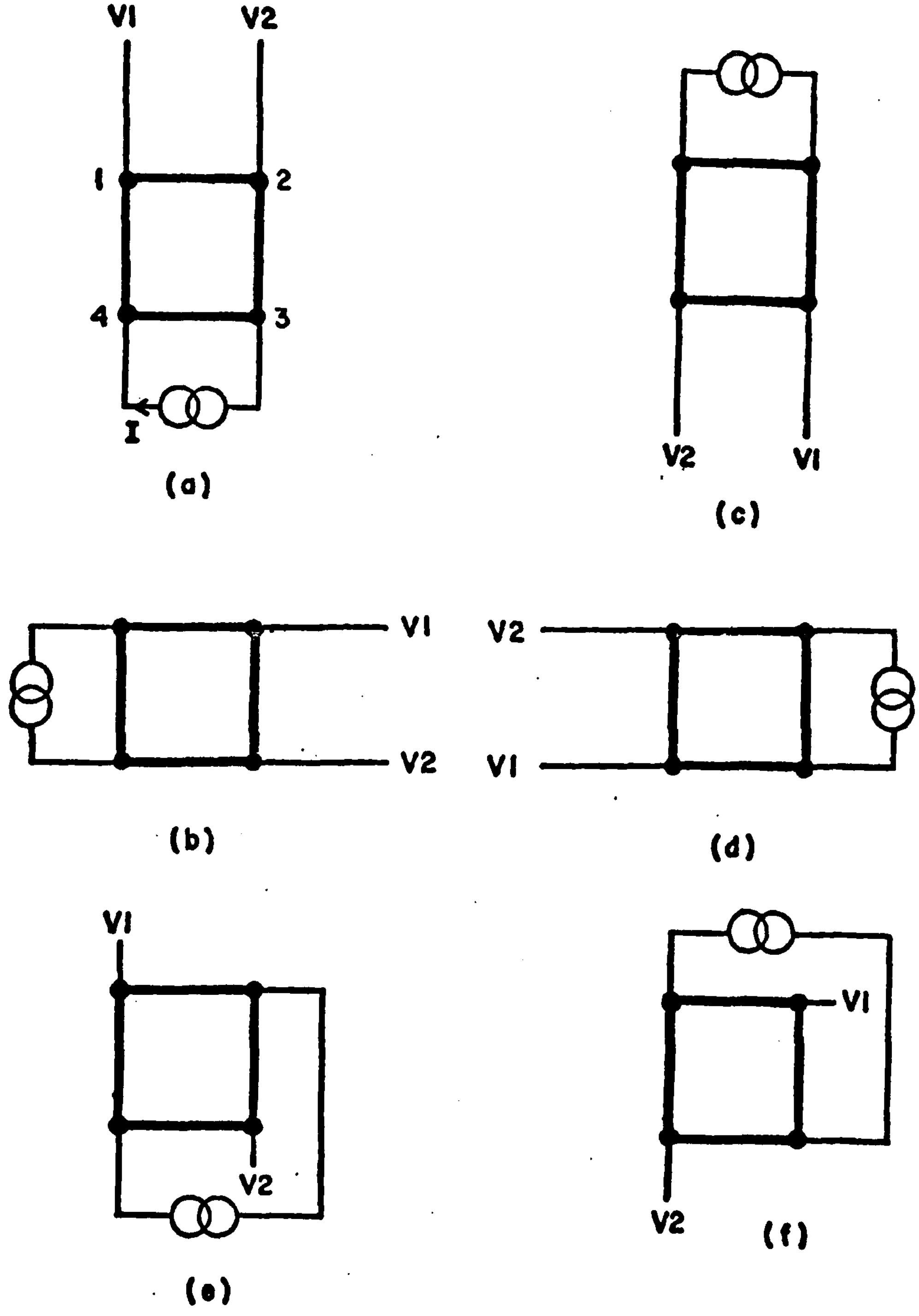

Figure 2. Illustration of the Sample Connections Used for Taking van der Pauw Transport Data

The sheet resistivity, ρ_s, in Ω/□ is calculated using Eq. (2);

$$\rho_s = \frac{\pi}{\ln 2} \left(\frac{R_a + R_b}{2}\right) f \left(\frac{R_a}{R_b}\right), \tag{2}$$

where R_a is a resistance in ohms defined for position (a) of Figure 2 as

$$R_a = (V1 - V2)/I \quad . \tag{3}$$

R_b is defined in a similar way for position (b), $f(R_a/R_b)$ is a geometrical correction factor dependent only upon the ratio of R_a and R_b, and I is the current in amperes.

The sheet-Hall coefficient, R_{HS}, in ohms-square centimeter per volt-sec is given by Eq. (4),

$$R_{HS} = 10^8 \; (\Delta Re/B) \quad , \tag{4}$$

where B is the applied magnetic field in gauss and ΔRe is the change in the resistance of position (e) of Figure 2 when the magnetic field is applied perpendicular to the sample. Then the surface carrier concentration, N_S, in cm^{-2} is calculated from Eq. (5),

$$N_S = \frac{r}{e \, R_{HS}} \quad , \tag{5}$$

where e is the electronic charge in Coulombs and r is the Hall-to-drift mobility ratio, which is customarily taken to be unity. The Hall mobility, μ_H, in square centimeter per volt-sec is obtained by Eq. (6),

$$\mu_H = \frac{R_{HS}}{\rho_s} \quad . \tag{6}$$

Figure 3 illustrates schematically a fully guarded circuit for making van der Pauw measurements. The connections indicated correspond to configuration (a) of Figure 2, but all six configurations are conveniently achieved by means of a six-section, six-position rotary switch inserted between the dashed lines as indicated in Figure 3. Each section of the switch is responsible for one of the six functions V1, V2, ammeter, battery, ammeter relay, and battery relay, while the six positions of the switch correspond to (a) ∿ (f) of Figure 2.

A sample to be tested is mounted on the sample probe. Using indium solder, the sample is connected electrically to the leads on the probe which in turn lead to the measurement system. For samples to be profiled, the indium contacts are coated with black wax that has been diluted with trichloroethylene. This coating protects the contacts of the samples from the etchant used for chemical layer-removal during profiling. After mounting the sample on the probe, it is placed between the poles of an electromagnet which can produce a magnetic field of 8,100 gauss.

A block diagram of the automated Hall-effect/sheet-resistivity measurement system is shown in Figure 4. The system consists of a Digital Equipment PDP 11-03 computer, four Keithley Model 610CR electrometers operated as unit gain amplifiers, a Keithley Model 725 programmable current source, and a Keithley Model 6900 digital multimeter to measure voltages of the sample. The current through the

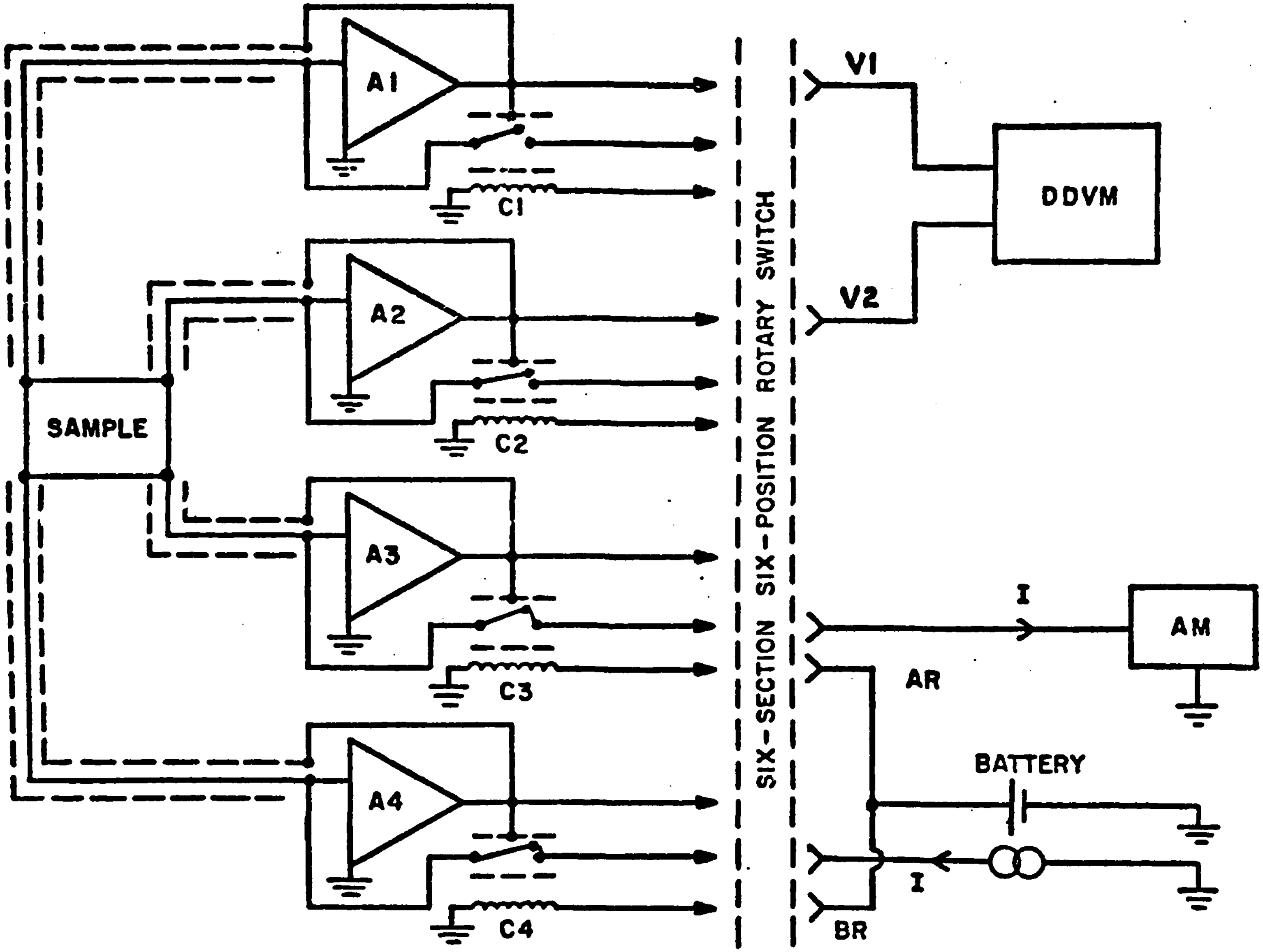

Figure 3. Schematic Diagram of the Hall-Measurement System for the Guarded van der Pauw Configuration

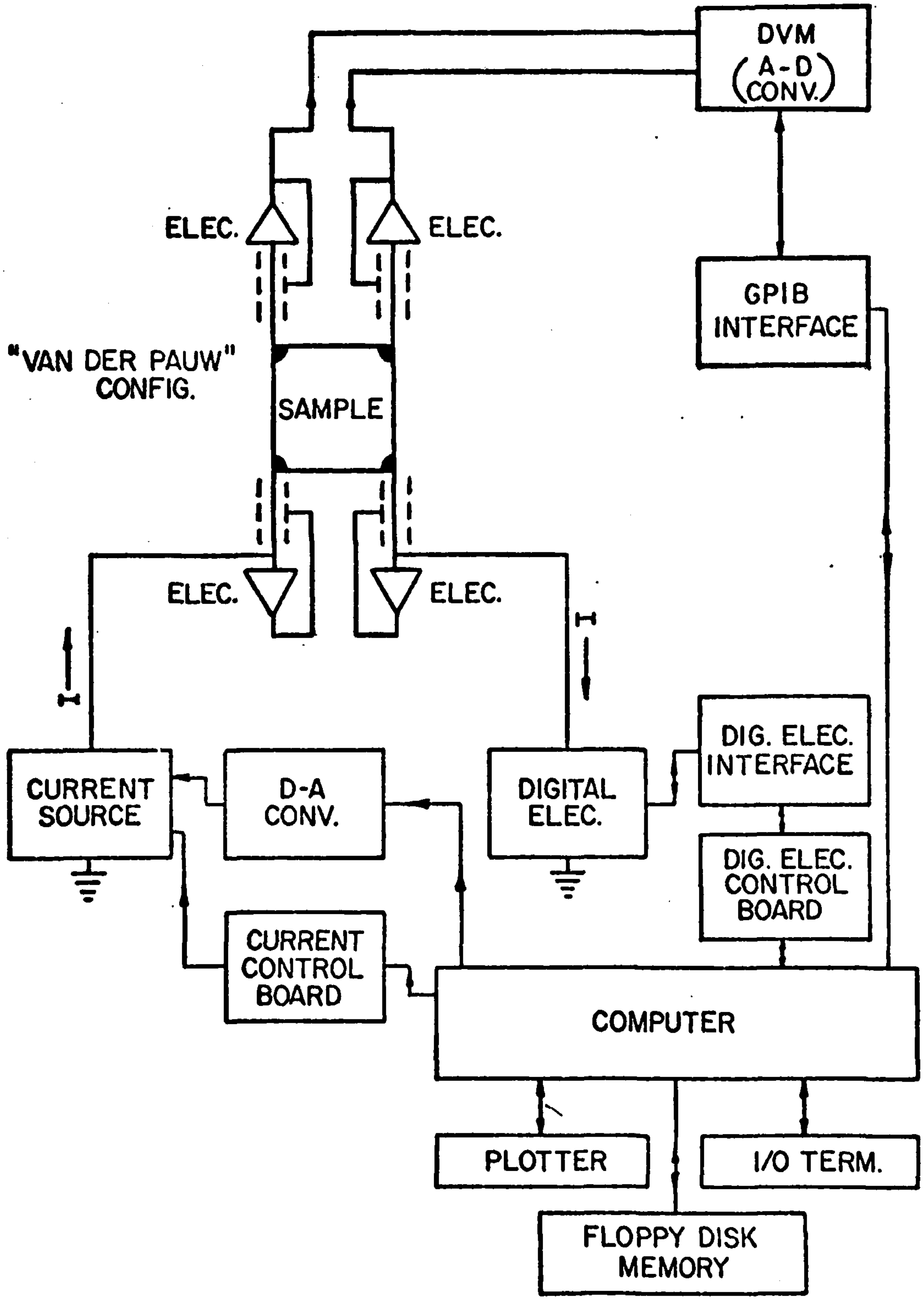

Figure 4. Block Diagram of Automated Hall-Effect/Sheet-Resistivity Measurement System

sample is read with a Keithley Model 616 digital electrometer (Ref 15).

Depth profiles to determine the carrier concentration N and Hall mobility μ_H are obtained by the combined use of the chemical layer-removal technique and Hall-measurements. The number of carriers N_i in the i^{th} layer and its Hall mobility $(\mu_H)_i$ can be obtained from the relations (Refs 8, 11, 16)

$$N_i = \frac{\Delta(\frac{1}{\rho_s})_i}{e(\mu_H)_i \, d_i} , \tag{7}$$

where $\Delta(\frac{1}{\rho_s})_i = \frac{1}{(\rho_s)_i} - \frac{1}{(\rho_s)_{i+1}}$ and d_i is the thickness of the i^{th} layer and

$$(\mu_H)_i = \frac{\Delta(\frac{R_{HS}}{\rho_s^2})_i}{\Delta(\frac{1}{\rho_s})_i} , \tag{8}$$

where $\Delta(\frac{R_{HS}}{\rho_s^2})_i = \frac{(R_{HS})_i}{(\rho_s)^2_i} - \frac{(R_{HS})_{i+1}}{(\rho_s)^2_{i+1}}$.

In the above equations, $(R_{HS})_i$ and $(\rho_s)_i$ are the sheet-Hall coefficient and the sheet resistivity, which are measured after removal of the i^{th} layer with thickness d_i.

Successive thin layers of the implanted section are removed using a diluted solution of H_2SO_4:30%H_2O_2:H_2O in a 1:1:100 ratio by volume at 0° C. Measurements are continued until all the active layers are removed. After completion of the profiling, the black wax is removed from the sample, and then the etched depth is measured. A typical etching rate is ∿100 Å/minute as determined by a Sloan-Dektak Surface Profile Measuring System. It has been assumed that the etching rate is constant in each etching.

IV. Experimental Results and Discussion

Electrical Activation

The results of Hall-effect/sheet-resistivity measurements made on Cr-doped GaAs substrates implanted with Si ions at an energy of 100 keV to doses ranging from 1 x 10^{12} to 1 x 10^{13} cm^{-2} and annealed at three different temperatures are shown in Figure 5. These results clearly show that the maximum electrical activation occurs at the 850° C anneal for all doses. The highest activation efficiency obtained was 89% for the sample implanted to a dose of 8 x 10^{12} cm^{-2}. The decrease in electrical activation at the 900° C anneal may be due to outdiffusion of implanted Si ions. For the sample implanted with 2 x 10^{12} cm^{-2} and annealed at 800° C, no appreciable electrical activation has been observed. Samples having a dose of 1 x 10^{12} cm^{-2} have also been investigated, but no measurable electrical activation was obtained even at the 900° C anneal. The annealing behavior of the Hall mobility indicates that mobilities obtained after the 850° C anneal increased significantly from the values of the 800° C anneal for all except the dose of 1 x 10^{13} cm^{-2}. However, the mobilities did not increase further after annealing the samples at 900° C. The mobilities for a dose of 1 x 10^{13} cm^{-2} remained about the same at three different annealing temperatures. Generally, mobilities

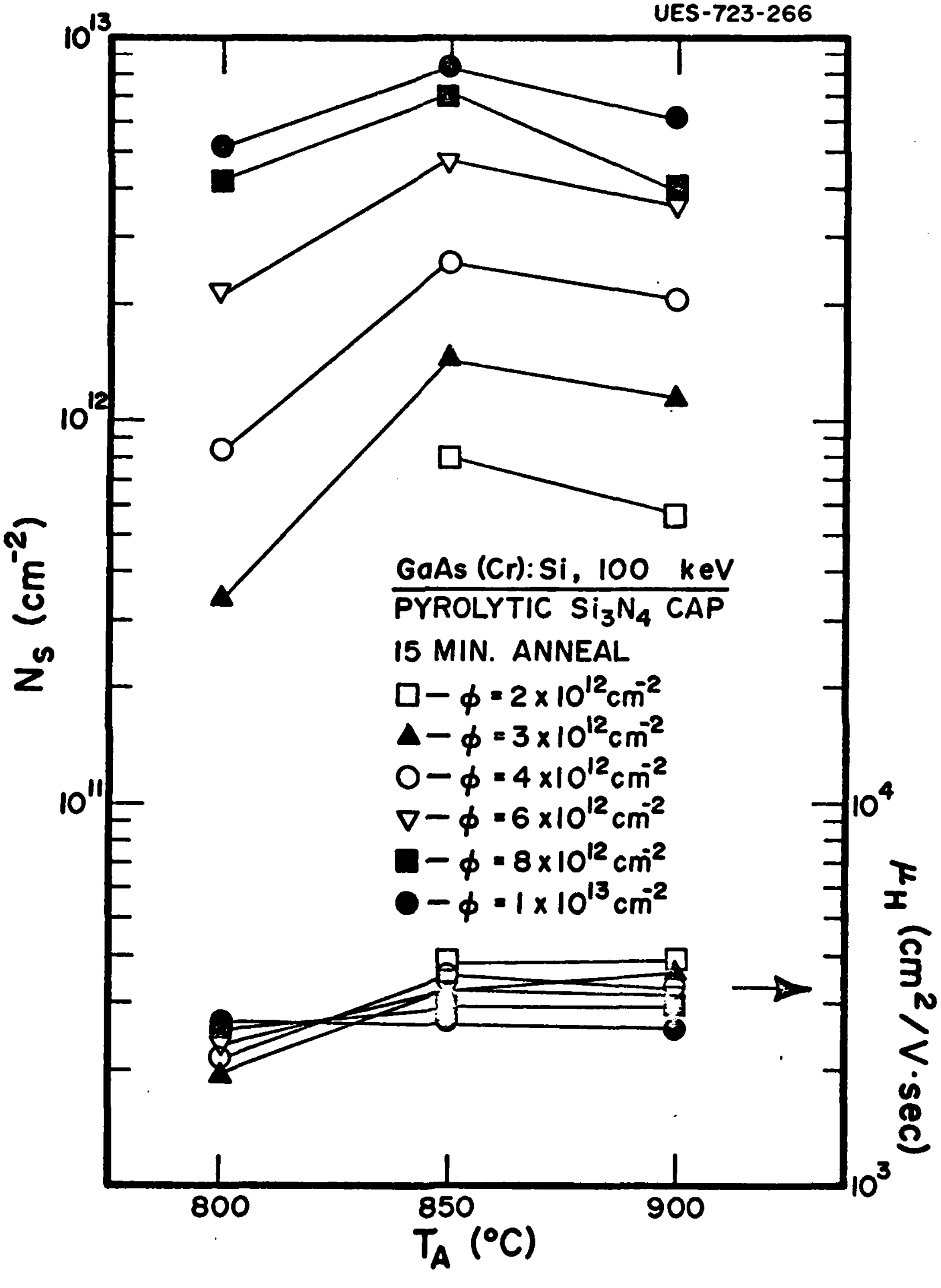

Figure 5. Surface-Carrier Concentration N_S and Hall Mobility μ_H versus Annealing Temperature T_A for 100-keV Si-Implanted Cr-Doped GaAs

are higher for low-dose samples than for high-dose samples.

Figure 6 is a replot of the data for Cr-doped substrates, showing surface carrier concentration versus implanted dose at different annealing temperatures. A straight line represents 100% activation efficiency. Activation efficiency clearly increases with ion dose up to 8 x 10^{12} cm^{-2} and decreases slightly at an ion dose of 1 x 10^{13} cm^{-2}. From this figure, we can deduce that the electrical activation for doses lower than 2 x 10^{12} cm^{-2} is very poor. The cut-off dose below which no appreciable electrical activation can be obtained is around 1 x 10^{12} cm^{-2}.

The results of Hall measurements made on undoped GaAs substrates implanted with Si ions are also shown in Figures 7 and 8. The maximum electrical activation occurs at the 850° C anneal for most doses as in the case of Cr-doped substrates. However, the surface carrier concentrations for doses of 3 x 10^{12} and 4 x 10^{12} cm^{-2} are nearly the same for three annealing temperatures. The activation efficiency increases with ion dose up to a dose of 6 x 10^{12} cm^{-2} except for the 800° C anneal, and then it decreases slightly with increasing dose. Electrical activation for the undoped GaAs substrates is, in general, slightly higher at all annealing temperatures than that for Cr-doped GaAs for doses up to 6 x 10^{12} cm^{-2}, whereas for higher doses, the activation is about the same for both substrates. The highest electrical activation efficiency obtained for undoped GaAs substrates was 87% for the sample implanted to a dose of 6 x 10^{12} cm^{-2}

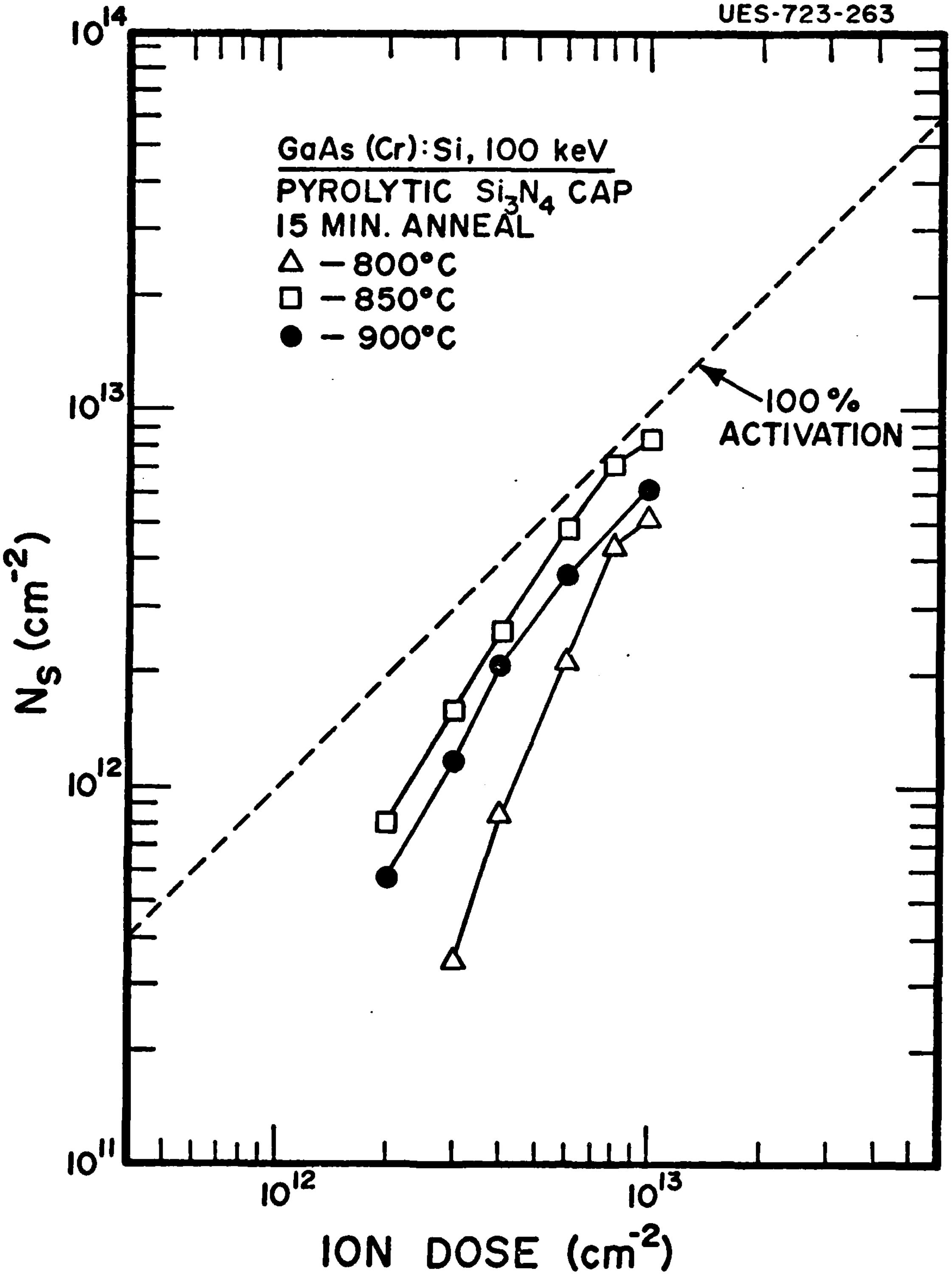

Figure 6. Surface-Carrier Concentration N_S versus Implanted-Ion Dose for 100-keV Si-Implanted Cr-Doped GaAs

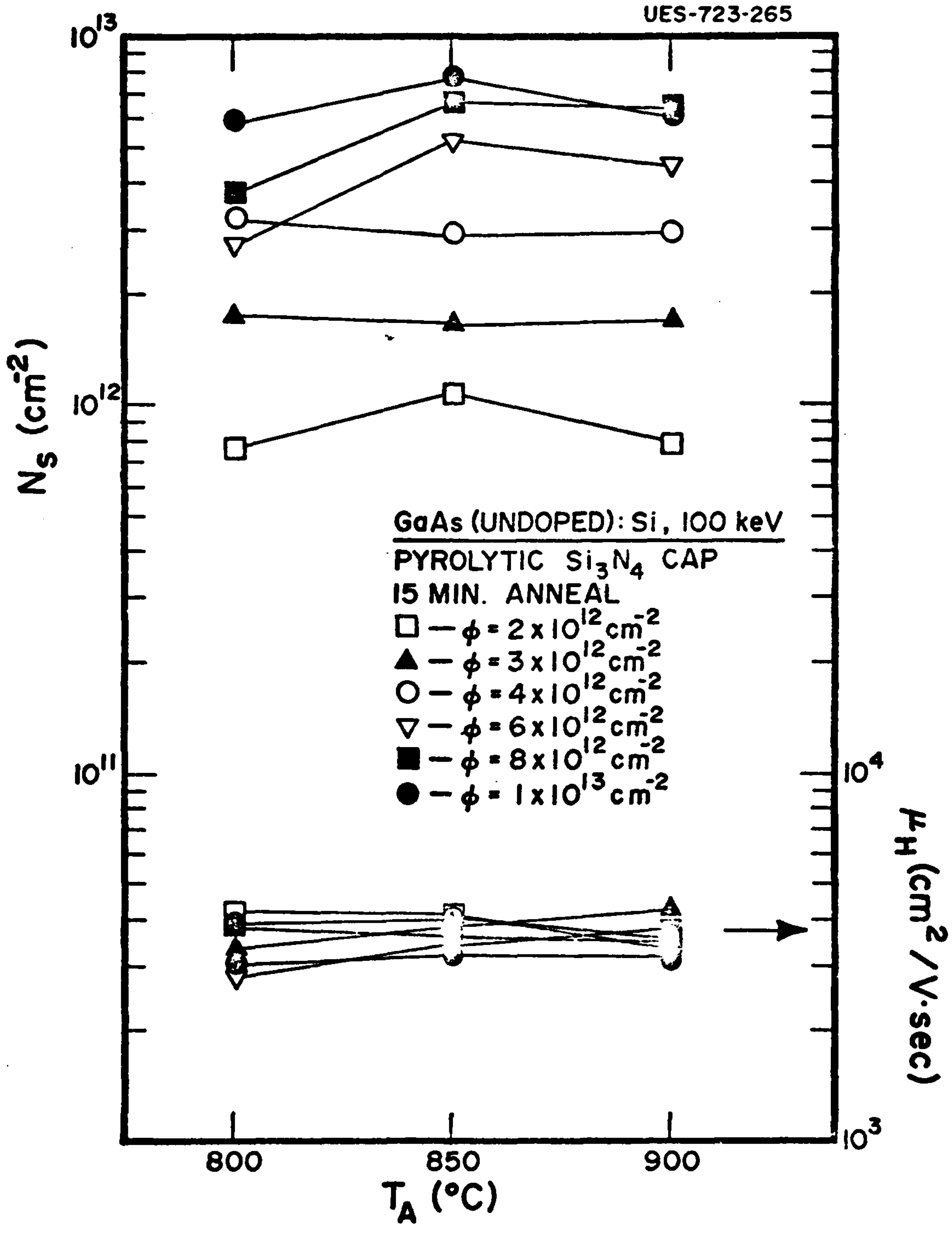

Figure 7. Surface-Carrier Concentration N_S and Hall Mobility μ_H versus Annealing Temperature T_A for 100-keV Si-Implanted Undoped GaAs

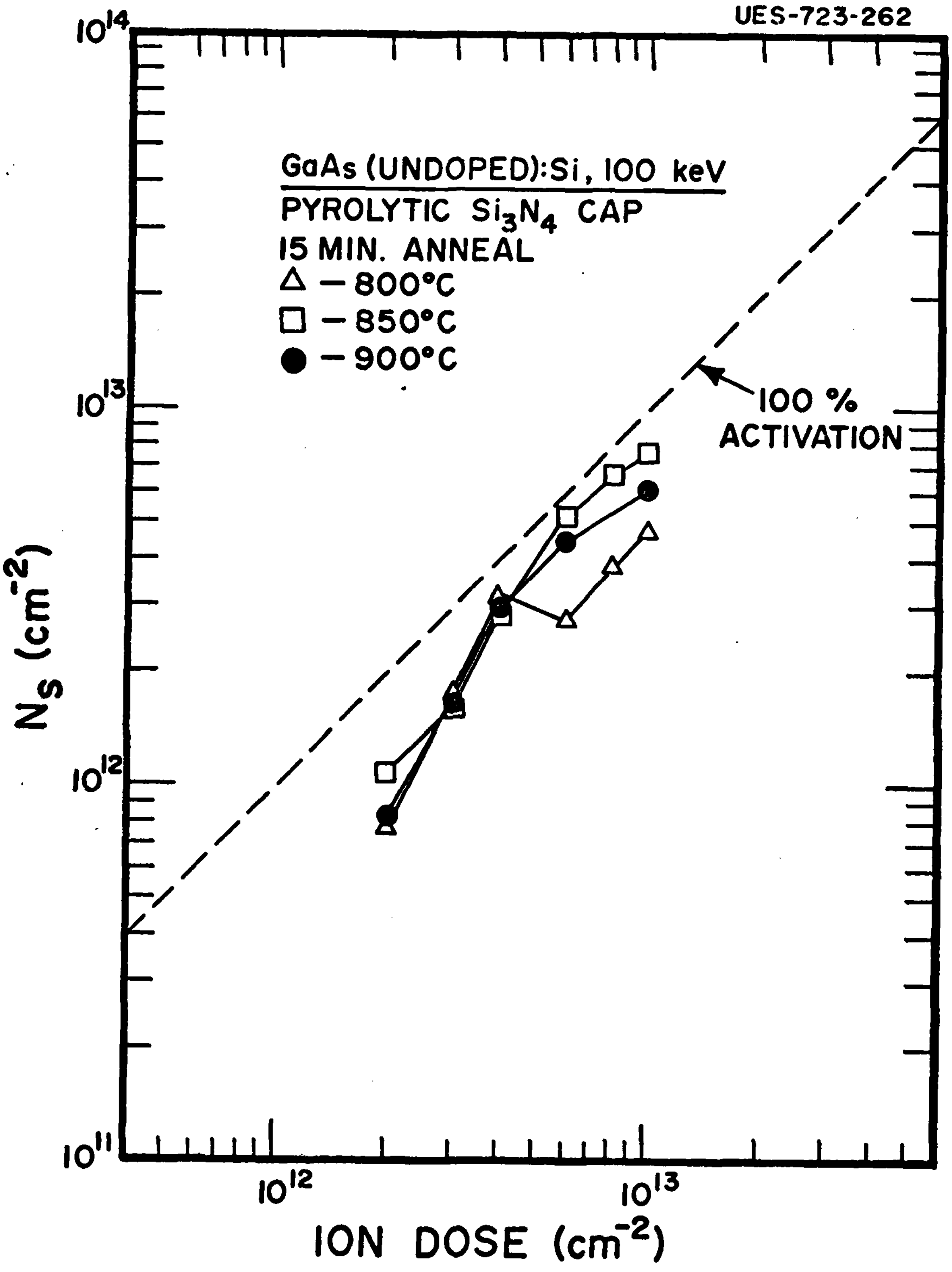

Figure 8. Surface-Carrier Concentration N_S versus Implanted-Ion Dose for 100-keV Si-Implanted Undoped GaAs

and annealed at 850° C. The annealing behavior of the Hall mobility indicates that mobility is nearly independent of annealing temperature. It seems that lattice damage due to ion bombardment can be annealed well even at around 800° C for these undoped GaAs substrates. Furthermore, the mobilities are considerably higher for undoped substrates than for Cr-doped substrates at all annealing temperatures and doses.

Since the optimum annealing temperature for most of the Si-implanted GaAs is 850° C, surface carrier concentrations obtained at the 850° C anneal have been compared for two different substrates, and the results are shown in Figure 9. For low-dose implants ($\leq 6 \times 10^{12}$ cm^{-2}), the electrical activation for undoped GaAs substrates is slightly better than for Cr-doped substrates, whereas for the two higher doses, the reverse is true. For both substrates, the electrical activation efficiency increases with ion dose up to about $6 \sim 8 \times 10^{12}$ cm^{-2}, and then it decreases with increasing ion dose.

Typical results of sheet resistivity ρ_s, Hall mobility μ_H, surface carrier concentration N_s, and electrical activation efficiency η for both Cr-doped and undoped GaAs substrates implanted with Si and annealed at three different temperatures are listed in Tables II and III, respectively.

The results of electrical measurements made on undoped GaAs substrates implanted with Si to an ion dose of 4×10^{12} cm^{-2} at various ion energies and annealed at 850° C are shown in Fig. 10. The electrical activation as well as the

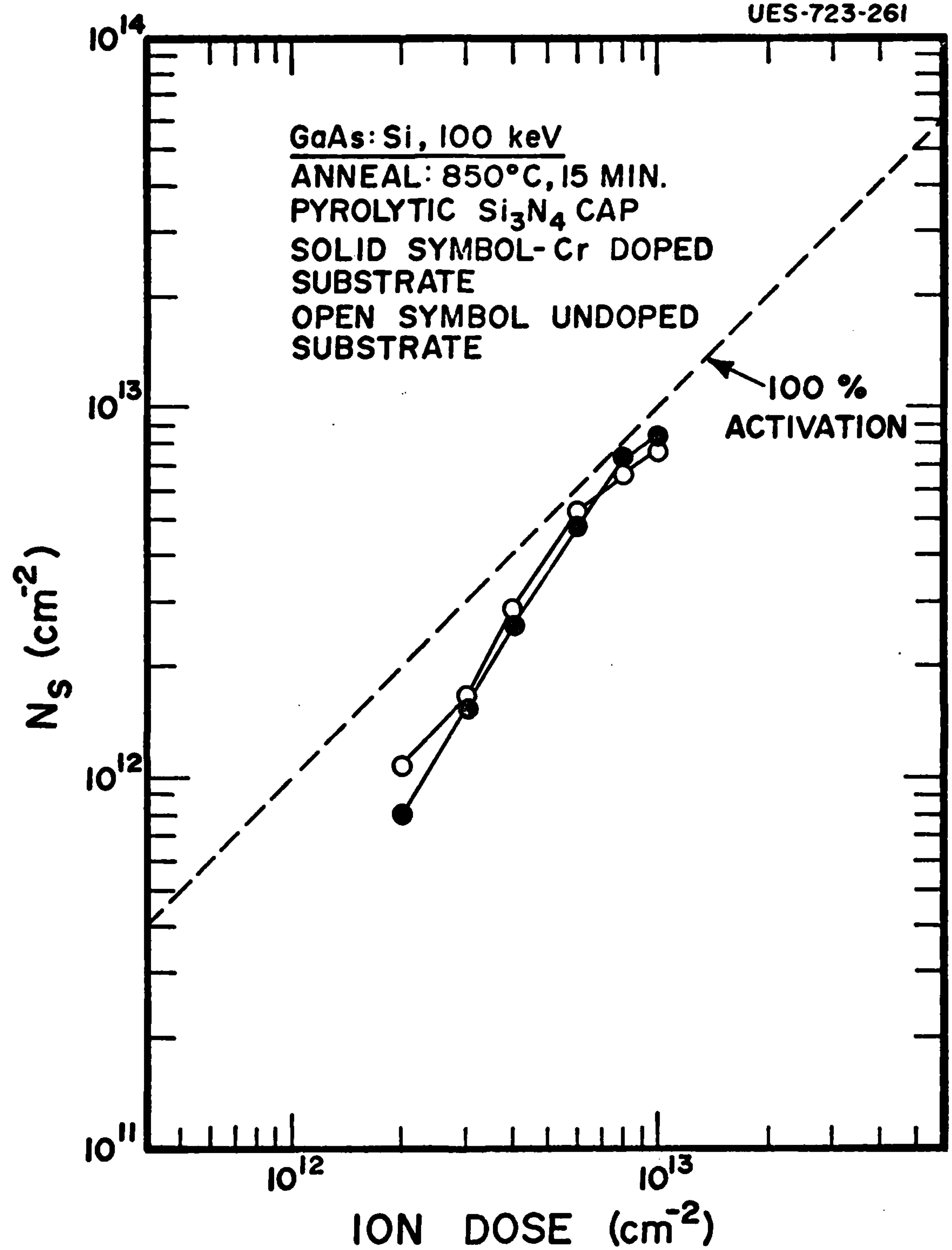

Figure 9. Surface-Carrier Concentration N_S versus Implanted-Ion Dose for Two Different GaAs Substrates Implanted with Si at 100 keV

Table II

Typical Results of Sheet Resistivity ρ_S, Hall Mobility μ_H, Surface-Carrier Concentration N_s, and Electrical Activation Efficiency η for Si-Implanted Cr-Doped GaAs Samples Annealed at Three Different Temperatures

Dose (cm^{-2})	T_A (°C)	ρ_s ($\Omega/\square$)	μ_H ($cm^2/V\cdot sec$)	N_s (carriers/$\square$)	η(%)
3×10^{12}	800	9.0×10^3	1998	3.5×10^{11}	11.6
4×10^{12}	800	3.5×10^3	2110	8.4×10^{11}	20.9
6×10^{12}	800	1.2×10^3	2319	2.2×10^{12}	36.1
8×10^{12}	800	5.8×10^2	2568	4.2×10^{12}	52.4
1×10^{13}	800	4.6×10^2	2650	5.2×10^{12}	51.5
2×10^{12}	850	2.0×10^3	3788	8.1×10^{11}	40.3
3×10^{12}	850	1.4×10^3	3247	1.4×10^{12}	47.6
4×10^{12}	850	6.9×10^2	3511	2.6×10^{12}	64.7
6×10^{12}	850	4.0×10^2	3233	4.8×10^{12}	80.2
8×10^{12}	850	3.0×10^2	2952	7.1×10^{12}	89.2
1×10^{13}	850	2.8×10^2	2652	8.3×10^{12}	83.3
2×10^{12}	900	2.8×10^3	3865	5.7×10^{11}	28.7
3×10^{12}	900	1.5×10^3	3598	1.2×10^{12}	39.1
4×10^{12}	900	9.0×10^2	3310	2.1×10^{12}	52.3
6×10^{12}	900	5.3×10^2	3227	3.7×10^{12}	61.0
8×10^{12}	900	5.2×10^2	2997	4.0×10^{12}	49.7
1×10^{13}	900	4.0×10^2	2575	6.1×10^{12}	60.9

Table III

Typical Results of Sheet Resistivity ρ_S, Hall Mobility μ_H, Surface-Carrier Concentration N_s, and Electrical Activation Efficiency η for Si-Implanted Undoped GaAs Samples Annealed at Three Different Temperatures

Dose (cm^{-2})	T_A (°C)	ρ_s ($\Omega/\square$)	μ_H ($cm^2/V \cdot sec$)	N_s (carriers/$\square$)	η(%)
2×10^{12}	800	1.9×10^3	4190	7.7×10^{11}	38.5
3×10^{12}	800	1.1×10^3	3340	1.8×10^{12}	58.3
4×10^{12}	800	5.1×10^2	3872	3.2×10^{12}	79.7
6×10^{12}	800	8.1×10^2	2790	2.8×10^{12}	45.9
8×10^{12}	800	4.4×10^2	3778	3.8×10^{12}	47.2
1×10^{13}	800	3.6×10^2	3034	5.8×10^{12}	57.6
2×10^{12}	850	1.4×10^3	4109	1.1×10^{12}	54.2
3×10^{12}	850	9.8×10^2	3841	1.7×10^{12}	55.0
4×10^{12}	850	5.6×10^2	3896	2.9×10^{12}	71.6
6×10^{12}	850	3.5×10^2	3467	5.2×10^{12}	86.9
8×10^{12}	850	2.6×10^2	3581	6.7×10^{12}	83.2
1×10^{13}	850	2.5×10^2	3241	7.6×10^{12}	76.4
2×10^{12}	900	2.3×10^2	3331	8.0×10^{11}	40.0
3×10^{12}	900	8.6×10^2	4251	1.7×10^{12}	56.7
4×10^{12}	900	6.0×10^2	3583	2.9×10^{12}	73.2
6×10^{12}	900	3.8×10^2	3754	4.4×10^{12}	73.9
8×10^{12}	900	2.8×10^2	3530	6.4×10^{12}	79.4
1×10^{13}	900	3.1×10^2	3291	6.1×10^{12}	61.0

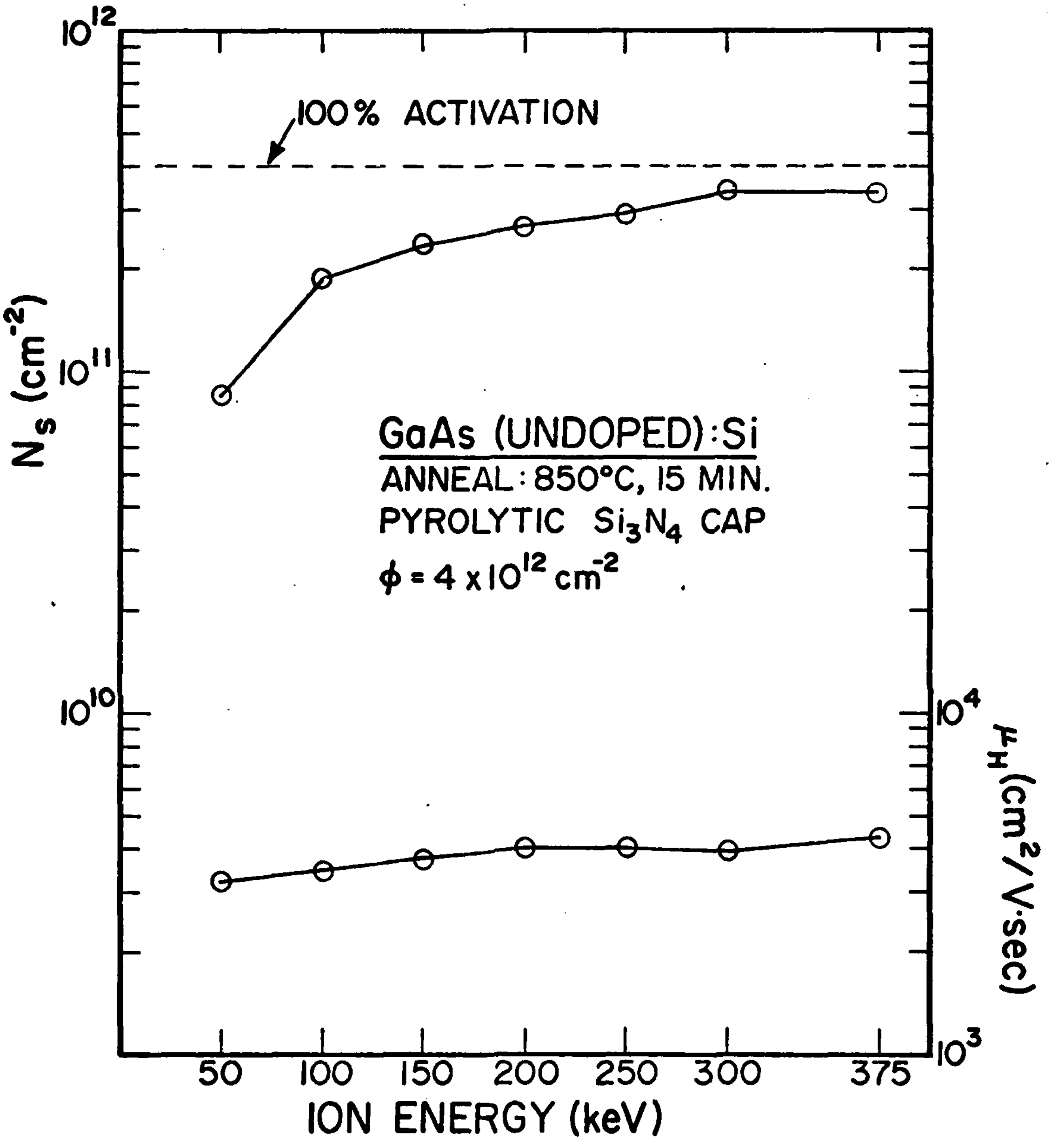

Figure 10. Surface-Carrier Concentration N_S and Hall Mobility μ_H versus Ion Energy for Si-Implanted Undoped GaAs

mobility for this dose level clearly increases with ion energy. This increase in electrical activation efficiency with ion energy may be attributed to the fact that less silicon outdiffusion is expected during the anneal of higher-energy implanted samples due to the greater implant depths which result compared to those obtained for lower-energy. The highest electrical activation efficiency obtained was 85% for an ion energy of 300keV.

Electrical Carrier Profiles

Electrical depth profiles of carrier concentration and Hall mobility for Cr-doped substrates implanted with Si at an ion energy of 100 keV and annealed at 850° C are shown in Figure 11 for the three lower dose samples. In the profile measurements, an annealing temperature of 850° C was especially chosen because the maximum electrical activation occurred at this temperature. The theoretical LSS profile for an ion dose of 4×10^{12} cm^{-2} is also shown in this figure for comparison. The theory predicts that the peak concentration will occur at ∿0.085 μm for an ion energy of 100 keV. For an ion dose of 3×10^{12} cm^{-2} or below, the profiles show no clear peaks and the active layers extend only to about 0.075 μm. Nearly all the Si ions in these active layers are electrically active, whereas the Si ions beyond the depth of about 0.075 μm are not electrically active at all or they are completely compensated. Therefore, the electrical activation efficiencies are about 40∿50% for these doses. Nevertheless, the maximum

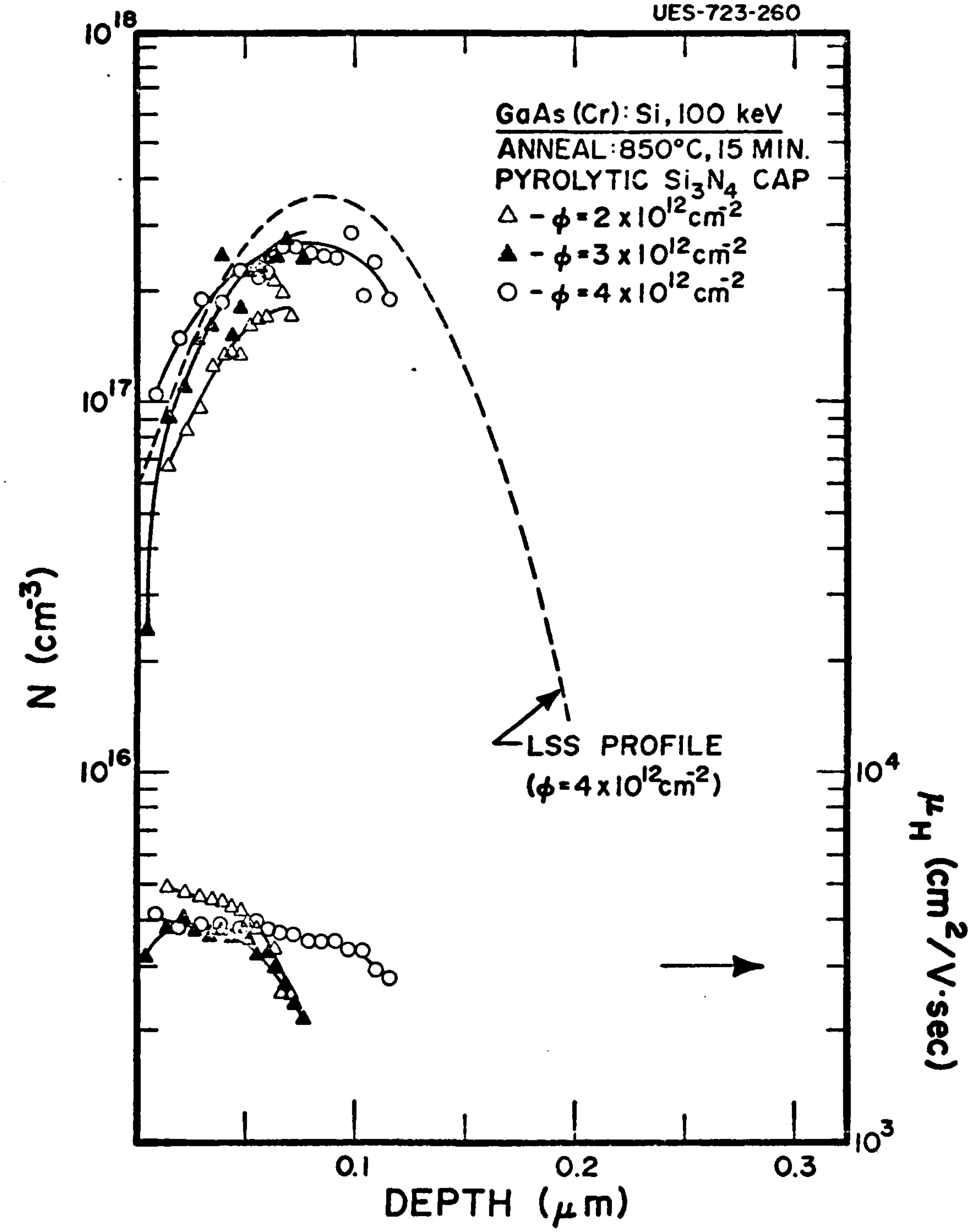

Figure 11. Carrier Concentration N and Hall Mobility μ_H Plotted as a Function of Depth for Three Lower-Dose Si-Implanted Cr-Doped GaAs

carrier concentrations obtained are about the same values predicted by the theory. The mobilities are high near the surface and they decrease rapidly as the depth increases. For a dose of 4 x 10^{12} cm^{-2}, the depth of an electrically active region is deeper than those for lower doses, extending roughly to 0.12 μm. The mobilities decrease gradually with increasing depth.

Electrical depth profiles of Si implants in Cr-doped GaAs substrates for three higher doses are shown in Figure 12. The LSS profile for a dose of 1 x 10^{13} cm^{-2} is also shown in this figure. For doses of 6 x 10^{12} and 1 x 10^{13} cm^{-2}, the carrier concentrations near the surface are higher than the values predicted by the theory, indicating a tendency of Si accumulation toward the surface. The carrier profile of a dose of 8 x 10^{12} cm^{-2} is much different from the others. The profile is much broader and the carrier-peak position is deeper than the LSS peak position. It also shows a slight indiffusion of the implanted Si ions. For a dose of 1 x 10^{13} cm^{-2}, the carrier profile follows generally very closely to the theoretical profile, and the peak-carrier concentration as well as the carrier-peak position agree very well with theory. The mobilities for these three doses are initially higher near the surface, and then decrease gradually with increasing depth.

Electrical depth profiles of carrier concentration and Hall mobility for undoped substrates implanted with Si to the three lower doses and annealed at 850° C are shown in Figure

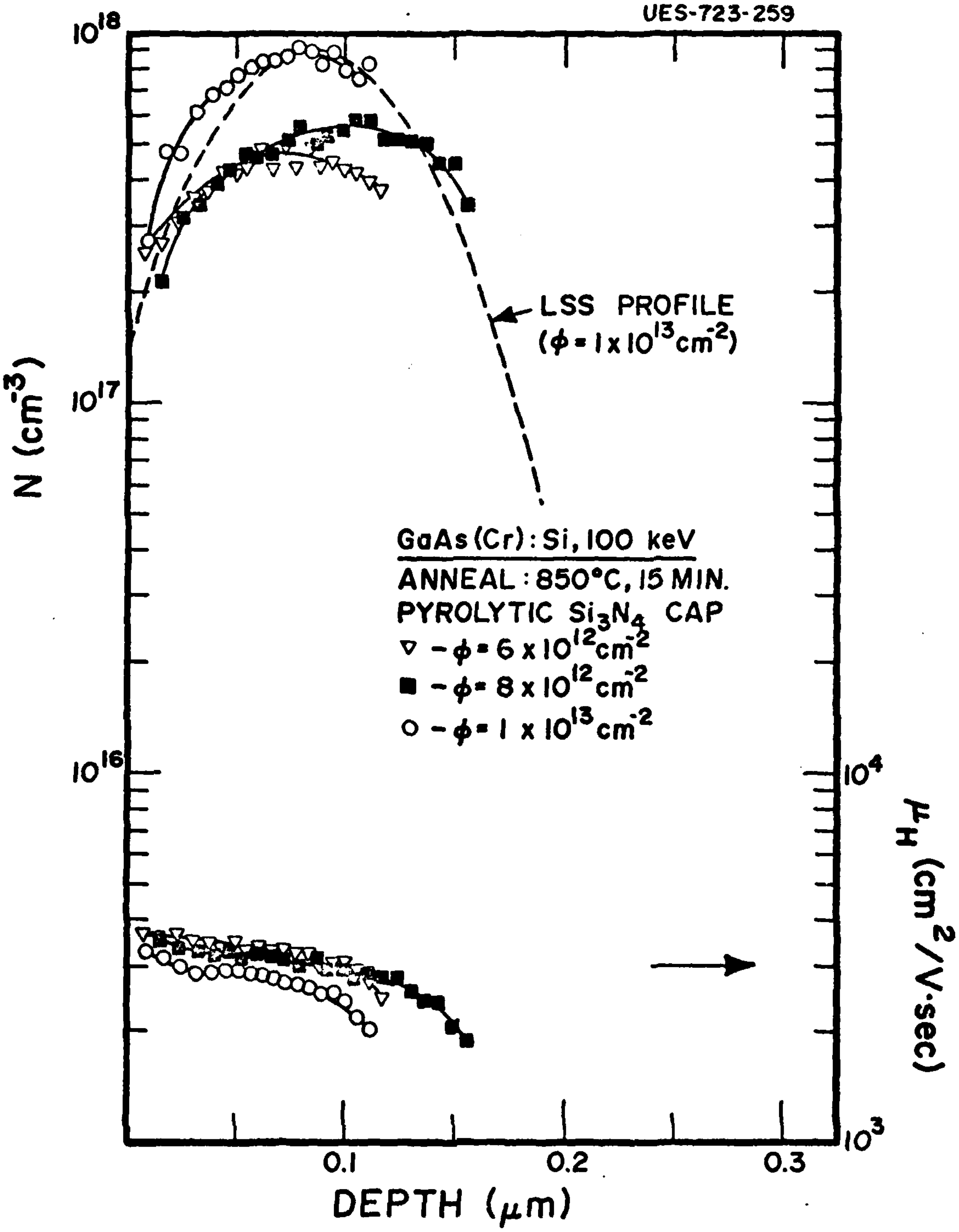

Figure 12. Carrier Concentration N and Hall Mobility μ_H Plotted as a Function of Depth for Three Higher-Dose Si-Implanted Cr-Doped GaAs

13. The LSS profile shown in this figure is for a dose of 4×10^{12} cm^{-2}. The shapes of the carrier profiles are quite different from one another. The carrier profile for a dose of 2×10^{12} cm^{-2} initially follows the LSS profile closely up to a few hundred angstroms. Thereafter, the carrier concentrations continue to increase with depth up to the end of the active layer. For the two higher doses, the positions of peak carrier concentrations are closer to the surface than those of the theoretical peak carrier concentrations. Also, the carrier concentrations near the surface are higher than the values predicted by the theory.

Electrical depth profiles of Si implants in undoped GaAs substrates for three higher doses are shown in Figure 14. The LSS profile for a dose of 1×10^{13} cm^{-2} is also shown in this figure for comparison. The carrier profiles for these doses extend deep into the sample, indicating a slight indiffusion of the implanted Si ions. Although the peak concentrations are much lower than the values predicted by the theory, the positions of peak-carrier concentrations agree very well with the position predicted by the LSS theory for all these doses. The mobilities decrease very slowly with increasing depth and the trends of the mobility-depth profiles are about the same for all three doses.

Electrical profiles of carrier concentration and Hall mobility for both Cr-doped and undoped GaAs substrates implanted with three doses of Si ions at an energy of 100 keV and annealed at 850° C are shown in Figure 15. It can be

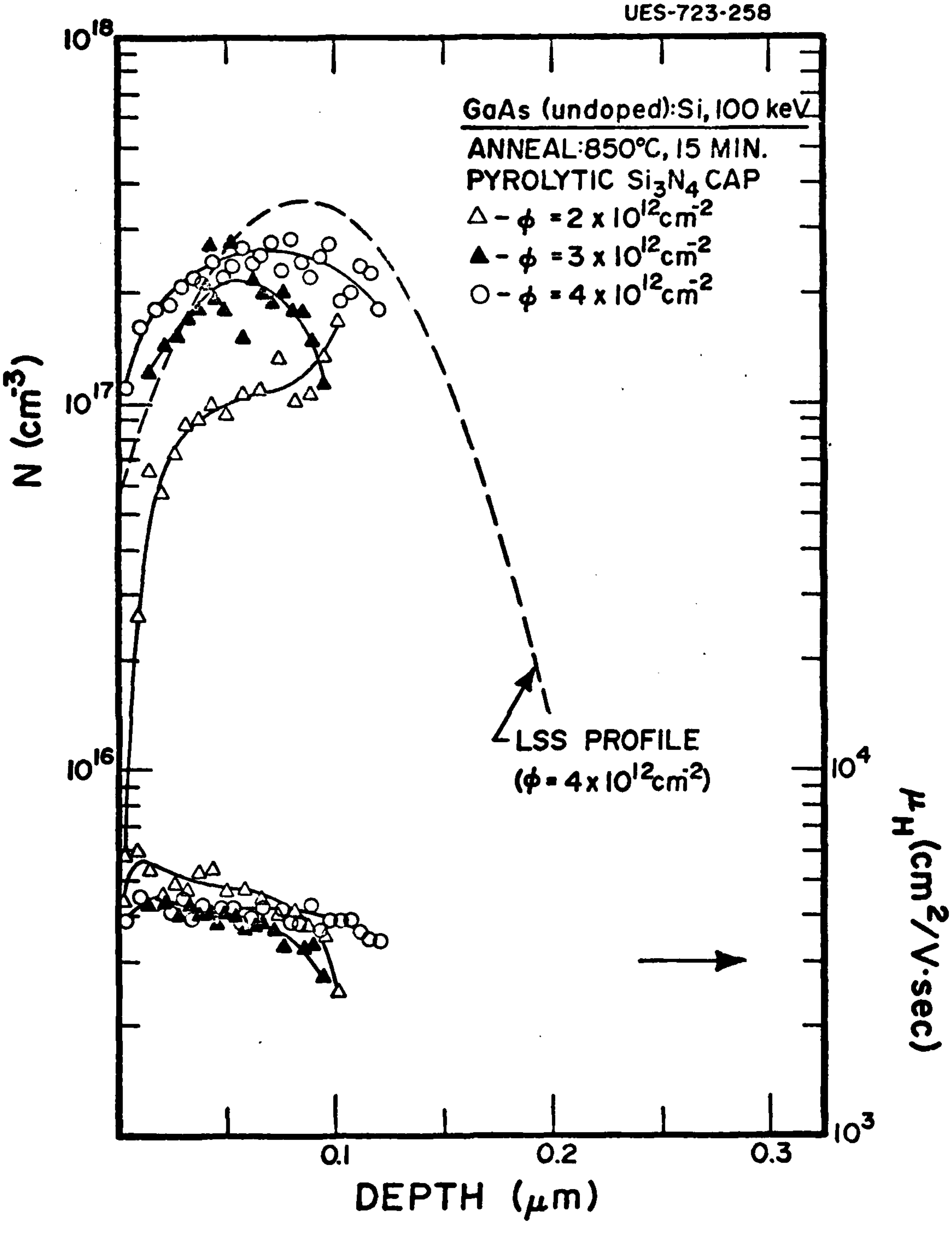

Figure 13. Carrier Concentration N and Hall Mobility μ_H Plotted as a Function of Depth for Three Lower-Dose Si-Implanted Undoped GaAs

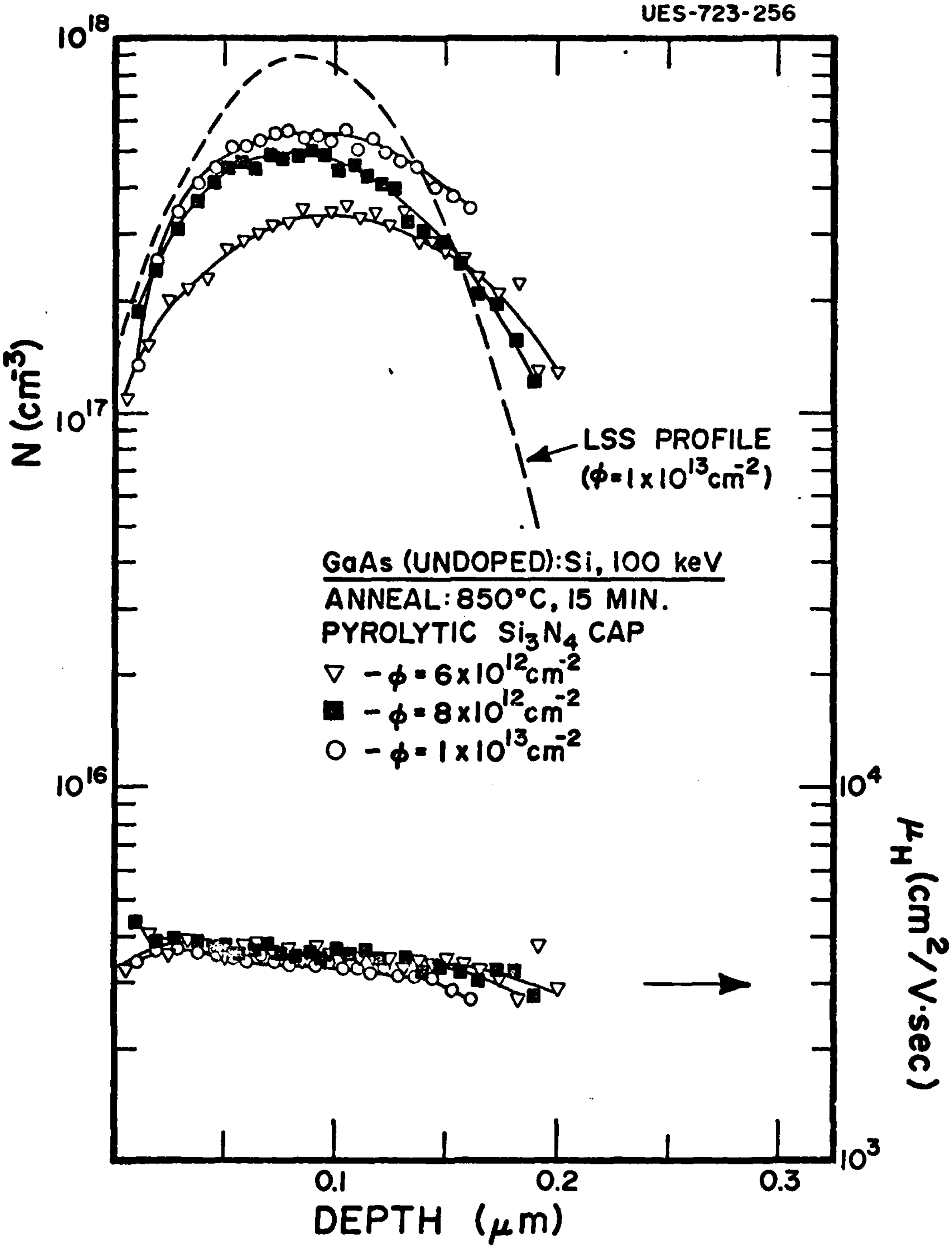

Figure 14. Carrier Concentration N and Hall Mobility μ_H Plotted as a Function of Depth for Three Higher-Dose Si-Implanted Undoped GaAs

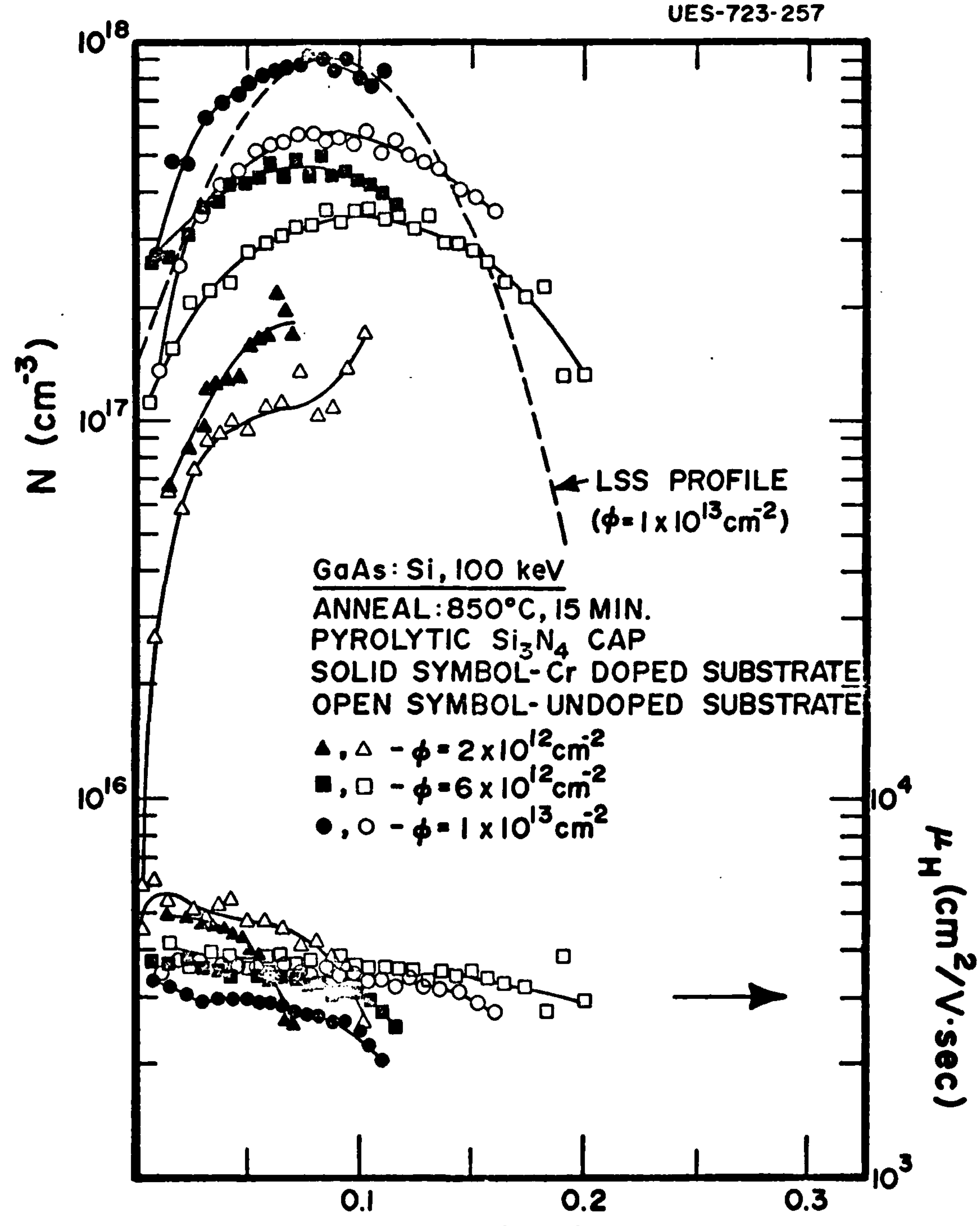

Figure 15. Carrier Concentration N and Hall Mobility μ_H Plotted as a Function of Depth for Two Different GaAs Substrates Implanted with Si at Various Ion Doses

clearly seen that the carrier concentrations in the Cr-doped substrates are higher than those in the undoped substrates throughout the entire active region for the given dose, whereas the reverse is true for mobilities. However, the depths of electrically active layers for undoped substrates are greater than those of Cr-doped substrates at the given dose. It seems that the Si ions in the Cr-doped substrates have a tendency to move toward the surface, whereas the Si ions in undoped substrates have a tendency to move into the substrates. The shallower active layers of the Cr-doped substrates suggest that electrical compensation in the deep side of the sample is greater for the Cr-doped substrates than for the undoped substrates.

Depth profiles of the carrier concentration and Hall mobility for Cr-doped substrates implanted with Si to a dose of 6 x 10^{12} cm^{-2} and annealed at three different temperatures are shown in Figure 16. Carrier and mobility profiles are shown to be highly dependent upon the annealing temperature. The carrier concentration of the sample annealed at 850° C is significantly higher than those of the samples annealed at either 800 or 900° C. The carrier concentrations for the 800 and 900° C anneals increase with depth, and the profiles show no clear peaks. Both the carrier concentrations and mobilities of the sample annealed at 800° C are significantly lower than those of the sample annealed at 850° C. This indicates that significant implantation damage remains even after annealing at 800° C for this dose. The low activation

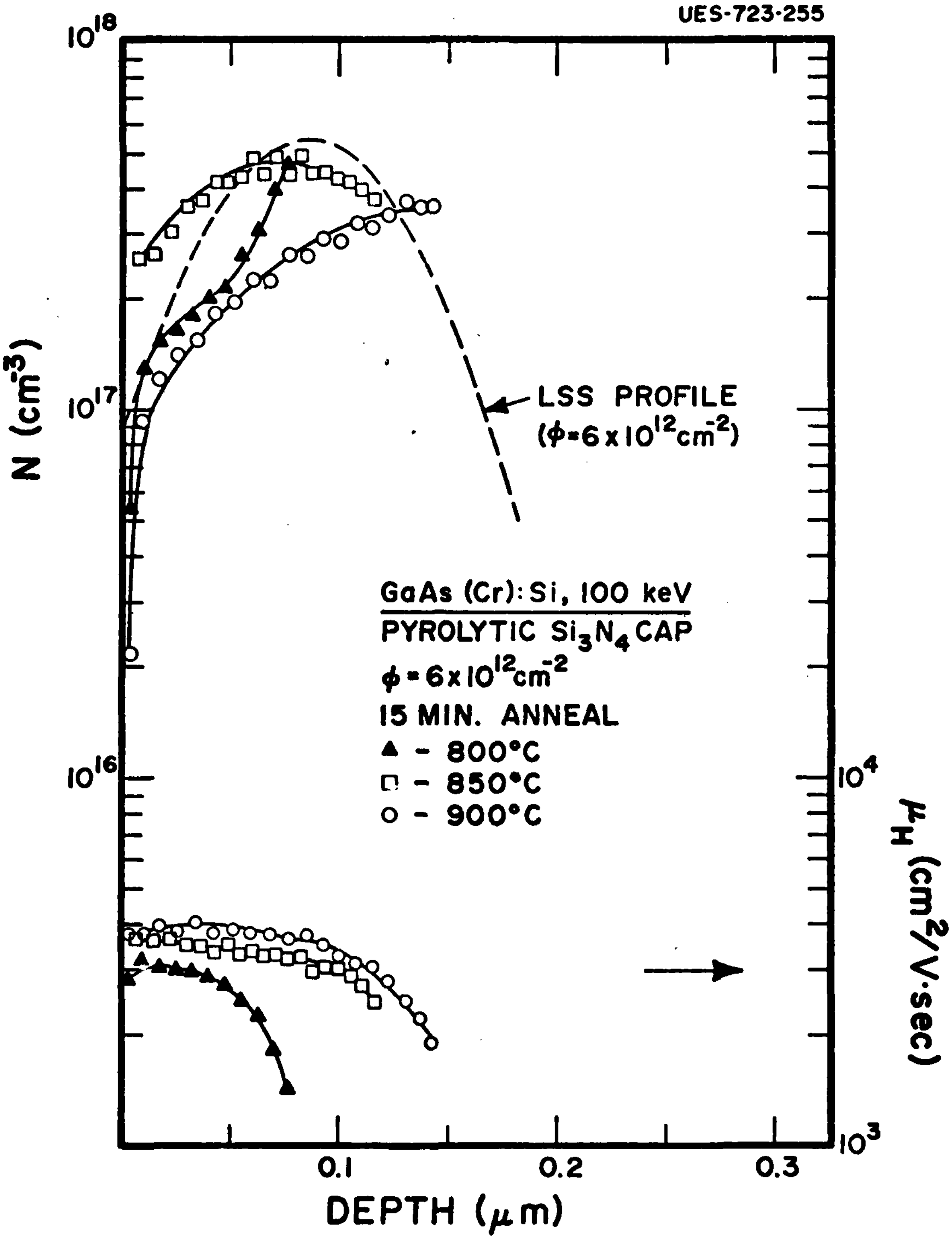

Figure 16. Carrier Concentration N and Hall Mobility μ_H Plotted as a Function of Depth for 100-keV Si-Implanted Cr-Doped GaAs Annealed at Different Annealing Temperatures

efficiency observed at this annealing temperature may be due to this unannealed damage. Also, the active region for the 800° C anneal is very shallow and no carriers are found beyond the projected range. The carrier concentrations of the sample annealed at 900° C are also very low compared with those of the 850° C anneal in most of the active region. This is probably due to outdiffusion of the implanted Si ions. Also, the profile for the 900° C anneal shows some indiffusion of Si ions.

Electrical profiles for undoped substrates implanted with Si to a dose of 6 x 10^{12} cm^{-2} and annealed at three different temperatures are shown in Figure 17. The carrier concentrations decrease with increasing annealing temperature. However, the active layer for the 800° C anneal is much shallower than those for higher temperature anneals, showing no carriers beyond around the projected range. The redistribution of the implanted Si ions takes place well into the damage-free region at an annealing temperature of 850° C or above, indicating a significant indiffusion of Si at this dose level. The carrier concentrations of the sample annealed at 900° C are much lower than those for an 850° C anneal, and this may be due to outdiffusion of the implanted Si ions. The mobilities for the 800° C anneal decrease sharply with increasing depth, whereas the mobilities for higher temperature anneal decrease gradually.

In order to provide some useful information to device designers, the maximum carrier concentration N_{max}, the

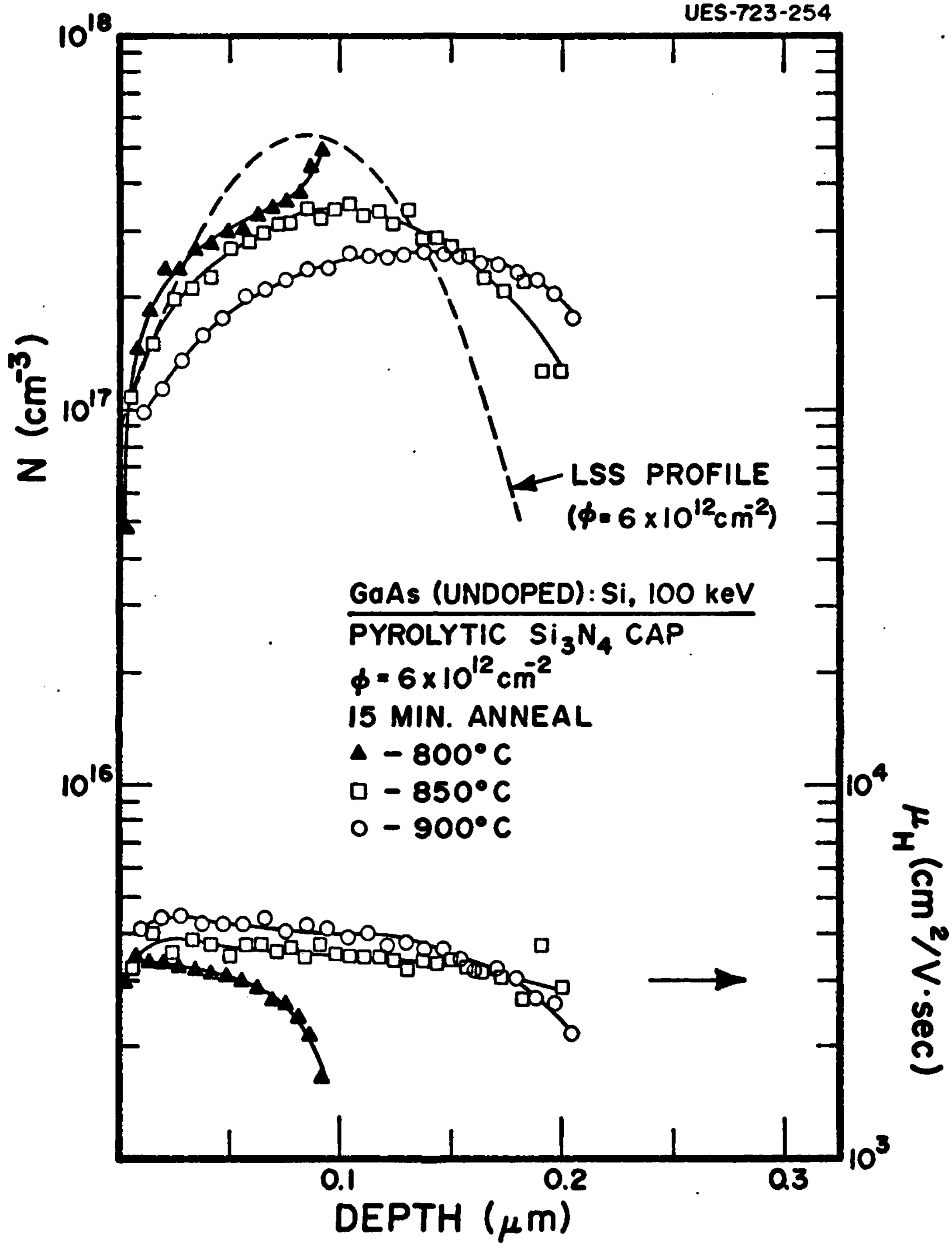

Figure 17. Carrier Concentration N and Hall Mobility μ_H Plotted as a Function of Depth for 100-keV Si-Implanted Undoped GaAs Annealed at Different Annealing Temperatures

carrier-peak position X_p, and the depth of the active layer of the 100 keV Si implants in Cr-doped and undoped GaAs substrates implanted to various ion doses and annealed at 850° C are summarized in Tables IV and V, respectively. Also, the peak-carrier concentrations and the projected range predicted by the LSS theory are listed in the tables for comparison.

Table IV

Summary of Maximum-Carrier Concentration N_{max}, Theoretical Peak-Carrier Concentration N_{max} of LSS, Carrier-Peak Position X_p, and Depth of the Active Layer for 100-keV Si Implants in Cr-Doped GaAs Substrates Annealed at 850° C for Various Ion Doses. The Projected Range for the 100-keV Si Implants in GaAs is 0.085 μm.

Ion Dose (cm^{-2})	N_{max} (cm^{-3})	N_{max} of LSS (cm^{-3})	X_p (μm)	Active Layer (μm)
2×10^{12}	2.1×10^{17}	1.8×10^{17}	0.063	0.070
3×10^{12}	2.8×10^{17}	2.7×10^{17}	0.073	0.077
4×10^{12}	2.9×10^{17}	3.6×10^{17}	0.097	0.115
6×10^{12}	5.0×10^{17}	5.4×10^{17}	0.083	0.116
8×10^{12}	5.9×10^{17}	7.2×10^{17}	0.105	0.156
1×10^{13}	9.2×10^{17}	9.0×10^{17}	0.078	0.111

Table V

Summary of Maximum-Carrier Concentration N_{max}, Theoretical Peak-Carrier Concentration N_{max} of LSS, Carrier-peak Position X_p, and Depth of the Active Layer for 100-keV Si Implants in Undoped GaAs Substrates Annealed at 850° C for Various Ion Doses. The Projected Range for the 100-keV Si Implants in GaAs is 0.085 μm.

Ion Dose (cm^{-2})	N_{max} (cm^{-3})	N_{max} of LSS (cm^{-3})	X_p (μm)	Active Layer (μm)
2×10^{12}	1.7×10^{17}	1.8×10^{17}	0.102	0.102
3×10^{12}	2.8×10^{17}	2.7×10^{17}	0.054	0.095
4×10^{12}	2.5×10^{17}	3.6×10^{17}	0.080	0.120
6×10^{12}	3.6×10^{17}	5.4×10^{17}	0.105	0.200
8×10^{12}	5.1×10^{17}	7.2×10^{17}	0.088	0.190
1×10^{13}	5.7×10^{17}	9.0×10^{17}	0.104	0.160

V. Conclusion

Through a comprehensive study of electrical properties of low-dose Si implants in both Cr-doped and undoped GaAs, it has been found that both electrical activation efficiency and carrier profiles are highly dependent upon the annealing temperature, the ion dose, and the type of substrate.

Although Si is an amphoteric dopant in GaAs, the results show that Si is exclusively an n-type dopant in GaAs at low doses. The optimum annealing temperature is found to be 850° C for all doses investigated. The electrical activation efficiencies increase with ion dose up to about $6\sim8 \times 10^{12}$ cm^{-2}, and then they decrease slightly at higher doses. The cut-off dose below which no appreciable electrical activation can be produced is around 1×10^{12} cm^{-2}. The highest electrical efficiency obtained for Cr-doped substrates was 89% for a dose of 8×10^{12} cm^{-2}, and that for undoped substrates was 87% for a dose of 6×10^{12} cm^{-2}. The electrical activations and mobilities of undoped GaAs are, in general, higher than those of Cr-doped GaAs at all annealing temperatures for a given dose. The electrical activations and mobilities also depend upon the ion energy for a given dose, and they increase with ion energy.

In general, the carrier profiles do not follow the theoretical LSS profiles. For a dose of 3×10^{12} cm^{-2} or

below, the active layers for both substrates are quite shallow, extending only to around the projected range.
Most carriers for Cr-doped substrates remain within the implanted region for all doses and annealing temperatures. However, slightly higher carrier concentrations than those predicted by theory are found near the surface region, indicating that the implanted Si ions have a tendency of moving toward the surface. The depth profiles of carrier concentrations for undoped GaAs implanted with higher doses ($\geq 6 \times 10^{12}$ cm^{-2}) are much broader than those for Cr-doped GaAs. The active layers of these samples extend deep into the sample, indicating a slight indiffusion of the implanted Si ions. Probably, the electrical compensation in the deep side of the sample is greater for the Cr-doped GaAs substrate than for the undoped. For a given dose, the carrier concentrations of the Cr-doped substrates are much higher than those of the undoped substrates, and the reverse is true for the mobility profiles. The carrier and mobility profiles for a dose of 6×10^{12} cm^{-2} show that significant implantation damage still remains even after the 800° C anneal. Also the profiles show that significant outdiffusion as well as indiffusion of the implanted Si ions occurs for the samples annealed at 900° C for both substrates. Therefore, the electrical activations obtained for the samples annealed at 800 and 900° C are much lower than those for the samples annealed at 850° C.

For further study, it is recommended that a comparative study of secondary ion mass spectroscopy (SIMS) atomic profiles and electrical carrier profiles is necessary in order to better understand the behavior of the silicon implants in GaAs. It may give useful information about the outdiffusion as well as indiffusion of implanted Si and the electrically inactive Si. Also, chromium redistribution in the Si-implanted Cr-doped GaAs samples will give some information about the electrical compensation. Further study of carrier profile dependence upon annealing temperature for both Cr-doped and undoped GaAs substrates implanted to different ion doses is also suggested to obtain more information about redistribution of the implanted Si ions. Electrical activation and carrier profile dependence upon ion energy as a function of annealing temperature may also be interesting because the activation efficiencies and the shapes of carrier profiles may significantly depend upon the implanted ion energy and annealing temperature.

Bibliography

1. J. P. Donnelly, W. T. Lindley, and C. E. Hurwitz. "Silicon- and Selenium-Ion-Implanted GaAs Reproducibly Annealed at Temperatures up to 950° C," Applied Physics Letters, 27(1): 41-43, 1 July 1975.

2. R. Kwor, et al. "Electrical Properties and Distribution of Sulfur Implants in GaAs," Journal of Applied Physics, 53(7): 4786-4792, July 1982.

3. K. Gamo, et al. "Selenium Implantation in GaAs," Solid State Electronics, 20: 213-217, 1977.

4. J. L. Tandon, M-A. Nicolet, and F. H. Eisen. "Silicon Implantation in GaAs," Applied Physics Letters, 34(2): 165-167, 15 January 1979.

5. J. D. Sansbury and J. F. Gibbons. "Conductivity and Hall Mobility of Ion-Implanted Silicon in Semi-Insulating Gallium Arsenide," Applied Physics Letters, 14(10): 311-313, 15 May 1969.

6. Y. K. Yeo, et al. "Amphoteric Behavior of Ge Implants in GaAs," Applied Physics Letters, 35(2): 197-199, 15 July 1979.

7. J. D. Sansbury and J. F. Gibbons. "Properties of Ion Implanted Silicon, Sulfur, and Carbon in Gallium Arsenide," Ion Implantation, 253-260, Gordon and Breach Science Publishers, Ltd., London, 1971.

8. L. J. van der Pauw. "A Method of Measuring the Resistivity and Hall Coefficient on Lamellae of Arbitrary Shape," Philips Technical Review, 20: 220-224, 1958.

9. L. J. van der Pauw. "A Method of Measuring Specific Resistivity and Hall Effect of Discs of Arbitrary Shape," Philips Research Reports, 13: 1-9, 1958.

10. P. M. Hemenger. "Measurement of High Resistivity Semiconductors Using the van der Pauw Method," Review of Scientific Instrumentation, 44(6): 698-700, June 1973.

11. N. G. E. Johansson, *et al*. "Technique Used in Hall Effect Analysis of Ion-Implanted Si and Ge," *Solid State Electronics*, *13*: 317-335, 1970.

12. G. Carter and W. A. Grant. "Ion Implantation of Semiconductors," Chap. 3, Edward Arnold, Ltd., London, 1976.

13. D. V. Morgan. "Prospects for Ion Bombardment and Ion Implantation in GaAs and InP Device Fabrication," *128*(4): Part I, *IEE Proc.*, August 1981.

14. J. F. Gibbons, *et al*. "Projected Range Statistics: Semiconductors and Related Materials," Dowden, Hutchinson and Ross, Inc., 1975.

15. Y. K. Yeo, *et al*. "Characterization of Ion-Implanted Semiconductors," Technical Report AFWAL-TR-80-1171: Avionics Laboratory, Wright-Patterson Air Force Base, Ohio, November 1980.

16. J. W. Mayer, et al. "Ion Implantation of Silicon," *Canadian Journal of Physics*, *45*: 4073-4089, 1967.

Appendix A

Table of LSS Range Statistics for Silicon Implants in GaAs

LSS RANGE STATISTICS FOR

SILICON IN GALLIUM ARSENIDE

SUBSTRATE PARAMETERS

	GALLIUM	ARSENIDE
Z	31	33
M	69.720	74.920
N	0.2214E 23	0.2214E 23
RHO/R	0.7973E 01	0.7523E 01
EPS/E	0.1350E-01	0.1277E-01
CNSE	0.1739E 02	0.1779E 02
MU	2.482	2.668
GAMMA	0.8188	0.7932

SNO 0.3851E 03

ION: SILICON

Z 14

M 28.086

ELECTRONIC CROSS SECTIONS OF LINDHARD,SCHARFF,SCHIOTT

ENERGY (KEV)	PROJECTED RANGE (MICRONS)	PROJECTED STANDARD DEVIATION (MICRONS)	THIRD MOMENT RATIO ESTIMATE	LATERAL STANDARD DEVIATION (MICRONS)	RANGE (MICRONS)	STANDARD DEVIATION (MICRONS)	NUCLEAR ENERGY LOSS (KEV/MICRON)	ELECTRONIC ENERGY LOSS (KEV/MICRON)
10	0.0103	0.0074	0.359	0.0097	0.0248	0.0069	0.4587E 03	0.1112E 02
20	0.0183	0.0125	0.285	0.0164	0.0412	0.0117	0.4860E 03	0.1573E 02
30	0.0262	0.0170	0.230	0.0226	0.0563	0.0159	0.4831E 03	0.1927E 02
40	0.0343	0.0213	0.180	0.0285	0.0709	0.0197	0.4715E 03	0.2225E 02
50	0.0424	0.0254	0.135	0.0343	0.0852	0.0233	0.4573E 03	0.2487E 02
60	0.0507	0.0294	0.094	0.0399	0.0993	0.0268	0.4420E 03	0.2724E 02
70	0.0592	0.0333	0.055	0.0454	0.1132	0.0300	0.4272E 03	0.2943E 02
80	0.0677	0.0370	0.020	0.0508	0.1270	0.0331	0.4131E 03	0.3146E 02
90	0.0763	0.0407	-0.014	0.0562	0.1407	0.0360	0.3998E 03	0.3337E 02
100	0.0850	0.0442	-0.046	0.0615	0.1543	0.0389	0.3873E 03	0.3519E 02
110	0.0937	0.0477	-0.075	0.0666	0.1677	0.0415	0.3756E 03	0.3689E 02
120	0.1025	0.0510	-0.104	0.0717	0.1811	0.0441	0.3646E 03	0.3853E 02
130	0.1113	0.0543	-0.131	0.0767	0.1944	0.0466	0.3543E 03	0.4011E 02
140	0.1202	0.0575	-0.156	0.0817	0.2076	0.0490	0.3447E 03	0.4162E 02
150	0.1291	0.0607	-0.181	0.0866	0.2207	0.0513	0.3356E 03	0.4308E 02
160	0.1380	0.0637	-0.205	0.0913	0.2337	0.0535	0.3270E 03	0.4449E 02
170	0.1470	0.0667	-0.227	0.0961	0.2466	0.0556	0.3190E 03	0.4586E 02
180	0.1559	0.0697	-0.249	0.1007	0.2594	0.0576	0.3114E 03	0.4719E 02
190	0.1649	0.0725	-0.270	0.1053	0.2721	0.0596	0.3042E 03	0.4849E 02
200	0.1735	0.0753	-0.290	0.1098	0.2848	0.0615	0.2974E 03	0.4975E 02
220	0.1918	0.0807	-0.329	0.1186	0.3097	0.0651	0.2847E 03	0.5217E 02
240	0.2097	0.0859	-0.366	0.1272	0.3344	0.0684	0.2733E 03	0.5449E 02
260	0.2276	0.0909	-0.400	0.1356	0.3586	0.0716	0.2629E 03	0.5672E 02
280	0.2455	0.0957	-0.432	0.1437	0.3826	0.0745	0.2534E 03	0.5886E 02
300	0.2632	0.1003	-0.462	0.1515	0.4061	0.0773	0.2447E 03	0.6092E 02
320	0.2809	0.1048	-0.491	0.1592	0.4294	0.0799	0.2366E 03	0.6293E 02
340	0.2985	0.1090	-0.519	0.1667	0.4523	0.0824	0.2291E 03	0.6485E 02
360	0.3160	0.1131	-0.545	0.1739	0.4750	0.0847	0.2222E 03	0.6674E 02
380	0.3334	0.1171	-0.570	0.1810	0.4973	0.0869	0.2157E 03	0.6857E 02
400	0.3507	0.1210	-0.595	0.1879	0.5193	0.0890	0.2097E 03	0.7035E 02
420	0.3679	0.1247	-0.618	0.1947	0.5411	0.0910	0.2040E 03	0.7209E 02
440	0.3850	0.1283	-0.641	0.2012	0.5626	0.0929	0.1987E 03	0.7379E 02
460	0.4020	0.1318	-0.663	0.2077	0.5838	0.0947	0.1937E 03	0.7544E 02
480	0.4185	0.1351	-0.684	0.2139	0.6048	0.0964	0.1890E 03	0.7707E 02
500	0.4357	0.1384	-0.705	0.2201	0.6255	0.0980	0.1845E 03	0.7865E 02
550	0.4772	0.1462	-0.753	0.2348	0.6763	0.1018	0.1742E 03	0.8249E 02
600	0.5181	0.1534	-0.798	0.2487	0.7256	0.1053	0.1654E 03	0.8616E 02
650	0.5582	0.1602	-0.841	0.2619	0.7737	0.1084	0.1574E 03	0.8968E 02
700	0.5978	0.1665	-0.880	0.2745	0.8205	0.1112	0.1502E 03	0.9307E 02
750	0.6367	0.1724	-0.918	0.2864	0.8662	0.1138	0.1438E 03	0.9633E 02
800	0.6750	0.1780	-0.954	0.2979	0.9109	0.1162	0.1379E 03	0.9949E 02
850	0.7127	0.1833	-0.988	0.3088	0.9545	0.1184	0.1326E 03	0.1025E 04
900	0.7498	0.1883	-1.021	0.3192	0.9972	0.1204	0.1277E 03	0.1055E 04
950	0.7864	0.1930	-1.053	0.3292	1.0391	0.1223	0.1232E 03	0.1084E 04
1000	0.8225	0.1975	-1.083	0.3388	1.0801	0.1241	0.1190E 03	0.1112E 04

Vita

Yong Yun Kim was born on 5 September 1952 in Seoul, Republic of Korea, the son of Woo Sun and Jong Su Kim. He graduated from high school in Seoul in 1971 and entered the Korea Military Academy from which he received the degree of Bachelor of Science in Mechanical Engineering in March 1976. Upon graduation he was commissioned in the ROKA. He immediately began active duty and served as Forward Observer Officer in Field Artillery. He also graduated from Seoul National University, from which he received the degree of Bachelor of Science in Physics. He then served as an Instructor for the Department of Electrical Engineering at the Korea Military Academy in Seoul until entering the Air Force Institute of Technology, School of Engineering, in June 1981.

Permanent Address: 154-7 Tongin-Dong Jongro-Ku
Seoul, Korea 110-00

UNCLASSIFIED

SECURITY CLASSIFICATION OF THIS PAGE (When Data Entered)

REPORT DOCUMENTATION PAGE

READ INSTRUCTIONS BEFORE COMPLETING FORM

1. REPORT NUMBER: AFIT/GEP/PH/82D-17

2. GOVT ACCESSION NO.: AD-A124 675

3. RECIPIENT'S CATALOG NUMBER:

4. TITLE (and Subtitle): ELECTRICAL PROPERTIES OF SILICON-IMPLANTED GaAs

5. TYPE OF REPORT & PERIOD COVERED: MS Thesis

6. PERFORMING ORG. REPORT NUMBER:

7. AUTHOR(s):

YONG YUN KIM
Captain ROKA

8. CONTRACT OR GRANT NUMBER(s):

9. PERFORMING ORGANIZATION NAME AND ADDRESS:

Air Force Institute of Technology (AFIT-EN)
Wright-Patterson AFB, Ohio 45433

10. PROGRAM ELEMENT, PROJECT, TASK AREA & WORK UNIT NUMBERS:

11. CONTROLLING OFFICE NAME AND ADDRESS:

Air Force Avionics Laboratory
(AFWAL/AADR)
Wright-Patterson AFB, Ohio 45433

12. REPORT DATE: December 1982

13. NUMBER OF PAGES: 59

14. MONITORING AGENCY NAME & ADDRESS (if different from Controlling Office):

15. SECURITY CLASS. (of this report): UNCLASSIFIED

15a. DECLASSIFICATION/DOWNGRADING SCHEDULE:

16. DISTRIBUTION STATEMENT (of this Report)

Approved for Public Release; Distribution Unlimited

17. DISTRIBUTION STATEMENT (of the abstract entered in Block 20, if different from Report)

18. SUPPLEMENTARY NOTES

Approved for public release: IAW AFR 190-17.
Lynn E. Wolaver
LYNN E. WOLAVER
Dean for Research and Professional Development
Air Force Institute of Technology (ATC)
Wright-Patterson AFB OH 45433

19 JAN

19. KEY WORDS (Continue on reverse side if necessary and identify by block number)

Gallium Arsenide	Surface Carrier Concentration	Profile
van der Pauw	Electrical Activation	Anneal
Ion Implantation	Mobility	
Cr-Doped	Silicon Implanted GaAs	
Undoped	LSS Theory	

20. ABSTRACT (Continue on reverse side if necessary and identify by block number)

A comprehensive study of the electrical properties of low-dose Si implants in both Cr-doped and undoped GaAs substrates has been made using the Hall-effect/sheet-resistivity measurement technique for various ion doses, ion energies, and annealing temperatures. The samples were implanted at room temperature and annealed with silicon nitride encapsulants in a hydrogen atmosphere for 15 minutes. N-type layers were produced at all dose levels investigated, and the optimum annealing temperature was 850° C for all

DD FORM 1 JAN 73 1473 EDITION OF 1 NOV 65 IS OBSOLETE

(continue

UNCLASSIFIED

SECURITY CLASSIFICATION OF THIS PAGE (When Data Ente

BLOCK 20: ABSTRACT (Cont'd)

doses. The highest electrical activation efficiencies obtained were 89% and 87% for Cr-doped and undoped GaAs substrates, respectively. The electrical activations and mobilities of undoped GaAs are, in general, higher than those of Cr-doped GaAs at all annealing temperatures for a given dose. The electrical activations and mobilities also depend upon the ion energy, and they increase with ion energy. Depth profiles of carrier concentrations and mobilities are highly dependent upon ion dose and annealing temperature. In general, the carrier profiles do not follow the theoretical profiles. The carrier profiles for undoped GaAs are much broader than those for Cr-doped GaAs. Significant implantation damage still remains after an 800° C anneal, and a 900° C anneal produces significant outdiffusion as well as indiffusion of the implanted Si ions.

END